STUDIES OF OPTO-ELECTRONIC SEMICONDUCTOR DEVICES AND SYSTEMS

by

D.A. Buchanan

A thesis
presented to the University of Manitoba
in partial fulfillment of the
requirements for the degree of
Master of Science
in
Electrical Engineering

Winnipeg, Manitoba, 1982

STUDIES OF OPTO-ELECTRONIC SEMICONDUCTOR DEVICES AND SYSTEMS

BY

DOUGLAS A. BUCHANAN

A thesis submitted to the Faculty of Graduate Studies of the University of Manitoba in partial fulfillment of the requirements of the degree of

MASTER OF SCIENCE

I hereby declare that I am the sole author of this thesis.

I authorize the University of Manitoba to lend this thesis to other institutions or individuals for the purpose of scholarly research.

D.A. Buchanan

I further authorize the University of Manitoba to reproduce this thesis by photocopying or by other means, in total or in part, at the request of other institutions or individuals for the purpose of scholarly research.

D.A. Buchanan

The University of Manitoba requires the signatures of all persons using or photocopying this thesis. Please sign below, and give address and date.

ABSTRACT

This thesis comprises two independent studies, which however both relate to the general area of semiconductor optoelectronic devices and systems :

1) A semiconductor device is proposed which provides for the modulation of the transmission of one optical signal, by means of a second optical (control) signal, having a different wavelength. The principle of operation of this device is that the electric field distribution in the semiconductor is photovoltaically modified by the absorption of the optical radiation in the control signal, and this in turn affects the absorption of a transverse optical beam by virtue of the Franz-Keldysh effect. The photon energy of the control beam is well in excess of the semiconductor energy gap ($\hbar\omega_1 >> E_{gap}$), whilst that of the controlled beam $\hbar\omega_2 \simeq E_{gap}$. Calculations for a GaAs opto-optic modulator indicate that the signal transmission of the controlled beam can be varied from approximately 0% to 100% for reasonable intensities of the control beam. This result is obtained for presently realizable semiconductor doping concentrations, and for reported spectral resolutions of single-mode $Al_xGa_{1-x}As$ laser sources.

2) Photoelectron counting distributions are obtained for sources which obey compound Poisson statistics. The sources (semiconductor lasers) emit coherent light and their intensity (Poisson rate parameter) fluctuates stochastically in accordance with a Gaussian distribution of temperatures. The lasers are otherwise assumed to be ideal and the quantum efficiency of the detector is assumed to be unity. This thesis represents an ideal situation where the source is the only concern in the calculation of the photoelectron counting distributions. It is found that for large temperature fluctuations ($\sigma > 10$ K) a substantial downward shift of the mean value of the photon probability density function is observed. The function becomes more asymmetric and the mean value decreases as the standard deviation of the temperature increases.

ACKNOWLEDGEMENTS

I would like to express my sincerest thanks to Professor H.C. Card for his guidance and his many helpful consultations without which I surely would never have completed this work. I would also like to acknowledge my colleagues in the Materials and Devices Research Group who contributed to my work here with their discussions and encouragement. A special thanks must also be extended to Dr.G. Troup and G. Gulak for their discussions on optics and photon statistics.

TABLE OF CONTENTS

LIST OF FIGURES

Figure

Chapter I

INTRODUCTION

In the rapidly advancing field of opto-electronics many new areas of engineering have been initiated. Data communications, for instance, has turned to fibre optic systems in hopes of increasing information capacity and data transmission rates. Even integrated technology has taken quantum leaps since the advent of very large scale (VLSI) and very high speed (VHSI) integration. Semiconductor lasers and other opto-electronic devices are now available and may in some cases be integrated to create a complete opto-electronic system on a single chip. Advances in planar wave and thin film fabrication technology have also had a dramatic impact in this area of research.

The intent of this thesis was to obtain a greater understanding of opto-electronic devices and systems, specifically devices fabricated from III-V compounds and systems utilizing fibre optics. During the course of the study of III-V compounds and integrated optic technology, an original theory for a novel opto-optic modulator was developed, and this is presented in the following chapter. This modulator is based on a photovoltaic Franz-Keldysh effect. It is suitable for applications in integrated optical switching or in optical logic devices.

Another consequence of our study of III-V compounds was the development of a useful statistical model of temperature effects in semiconductor lasers. There are many circumstances (i.e. long distance fibre optic transmission) where the detected intensity of the laser beam is very low. Subsequently photon statistics must be used. Under these conditions, temperature variations can have a dramatic effect on the statistics and therefore on the information in the detected radiation. This study of compound Poisson statistics associated with the temperature variations in semiconductor lasers at low detected intensities is presented in Chapter III.

The final subject addressed in this thesis is an experimental investigation of the spectral characteristics of a fibre optic system. A short range, inexpensive system was chosen (i.e. Hewlett-Packard HBFR-0500). This system included an LED transmitter, an integrated reciever and a 5 meter length of plastic fibre (attenuation 0.6 dB/m). The spectral response of the source and the fibre were determined in order to assess the component match in this design. Since this study, unlike the two investigations described above, did not involve original research, the results are presented in the Appendix to this thesis.

The final chapter relates the conclusions of the above studies.

Chapter II

OPTO-OPTIC MODULATOR BASED UPON A PHOTOVOLTAIC FRANZ-KELDYSH EFFECT IN SEMICONDUCTORS*

2.1 INTRODUCTION

Electro-optic and acousto-optic modulators are well known devices with many applications in optical signal processing. This thesis proposes an alternative device structure based upon the optically-controlled modulation of the optical absorbtion in a semiconductor, which we term an opto-optic modulator.

The dependence upon an electric field of the optical absorption coefficient of a semiconductor was originally studied by Franz [2] and Keldysh [3]. It was shown that in the presence of an electric field, optical absorption occurs at photon energies lower than the energy gap. Theoretical developements in modeling this effect have been presented by Calloway [4,5]. Experimental results by Moss [6] ,Lambert [7] and others have shown good quantitative agreement with the theory.

---

* The contents of this chapter have been submitted for publication [1]

The photovoltaic effect in semiconductor devices, such as pn junctions or Schottky barriers, produces an open circuit voltage across the (unconnected) device when an optical signal is incident upon its surface. This open-circuit voltage reduces the diffusion potential and therefore the electric field in the space-charge region adjacent to the junction. In this thesis we propose to exploit this photovoltaic modification of the electric field distribution to control the absorption of an optical signal by means of the Franz-Keldysh effect.

This second optical beam which more effectively penetrates the semiconductor sample will be absorbed to a degree dependent upon the intensity of the primary optical excitation. One is then able to modulate the absorption of one optical signal by the use of another.

For applications in integrated optics, a system that pre-empts the normal intermediate role of electrical signals would be of great benefit in improving realizable information processing capacity of digital systems.

2.2 THEORY

It has been shown that for photon energies in the vicinity of the energy gap there is a substantial increases in the optical absorption coefficient associated with a shift to lower energies of the optical absoption edge, in the presences of a strong electric field. The required magnitude of

electric field may be realized in the space-charge (or depletion) region of a semicondictor junction or interface device. If an optical signal (of photon energy well in excess of the energy band gap) is absorbed and modifies the field by virtue of the photovoltaic effect, the absorption of an independent optical beam with approximately bandgap photon energy can be controlled. This gives rise to an optically controlled optic-modulator.

The energy band structure of a semiconductor under an appreciable electric field [9] is shown in Fig. 2.1 . The conduction and valence bands are tilted to such a degree that the electron wavefunctions corresponding to these two bands penetrate into the forbidden energy gap. It is then possible for a photon with energy ($\hbar\omega$) less than that of the energy gap to become absorbed and thereby produce an electron-hole pair. This is known as the Franz-Keldysh effect [2,3]. This effect has been employed in electro-optic modulators in which the applied voltage controls the optical absorption properties of the semiconductor.

Figure 2.2 (a) shows the band structure of a Schottky barrier device, both in the dark (solid line) and under illumination (broken line). The Schottky barrier is simply a metal-semiconductor contact which when connected in an electrical circuit exhibits rectifying properties. In the present application however the terminals are left in the open circuit condition. A space-charge (depletion) region exists

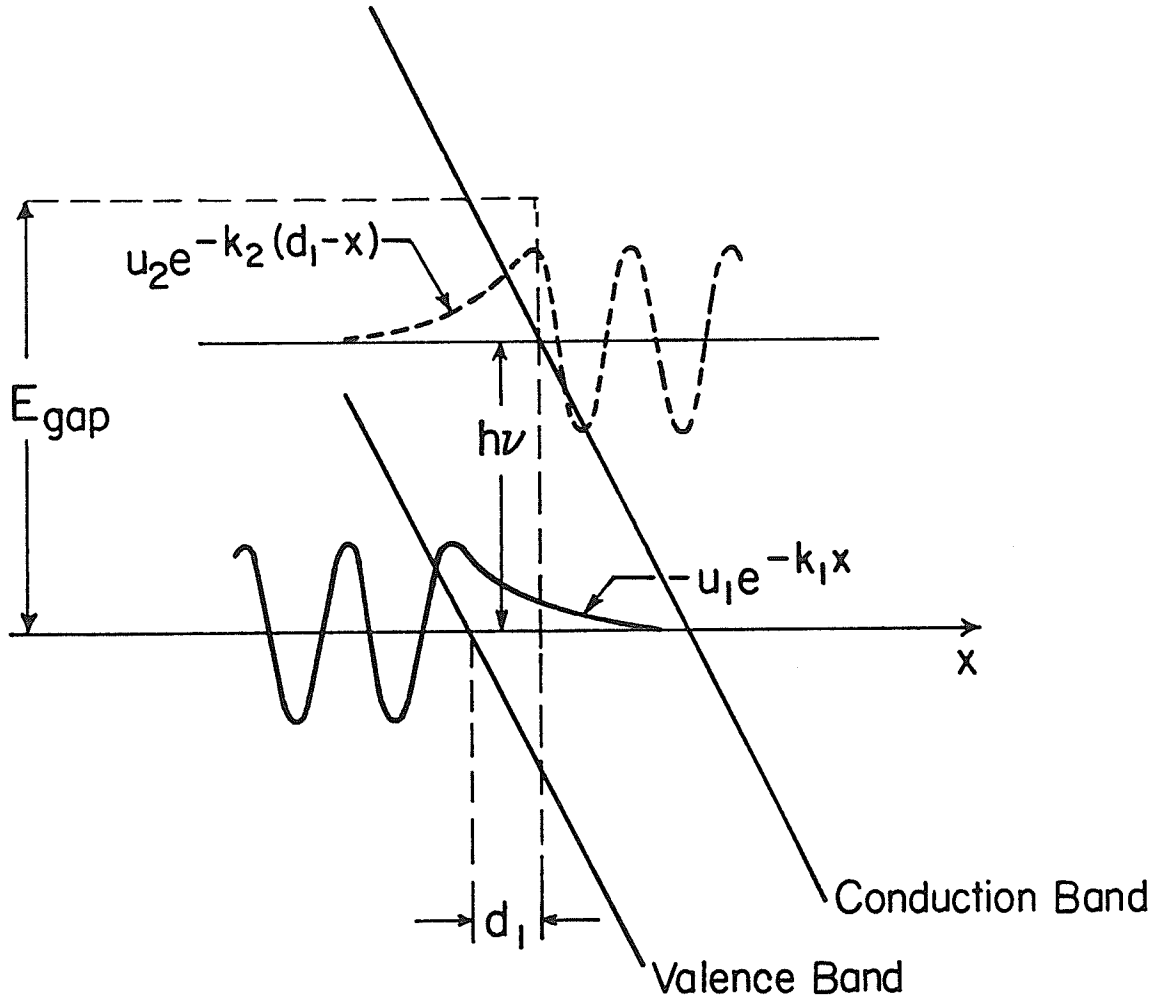

Figure 2.1: Energy band diagram of a semiconductor in the presence of a strong electric field.

exists in the semiconductor surface region. In the depletion approximation [10], the electric field can be assumed to be linear throughout the space-charge region provided the impurity doping concentration is independent of position. Under strongly absorbed optical illumination the width of the space-charge region is reduced and with it the magnitude of the electric field as shown in Fig. 2.2 (b).

The maximum (surface) electric field ε_{max} and the space charge width (W) depends upon the barrier height (ϕ_b) , which determines the built-in (diffusion) potential V_d in Fig. 2.2, and upon the open circuit voltage which is dependent upon the intensity of the absorbed optical radiation. The doping concentration determines the bulk Fermi potential (ϕ_n) given by [11]

$$\phi_n = V_T \ln \left(\frac{N_c}{N_d} \right) \tag{2.1}$$

assuming an n-type semiconductor, where

$V_T = kT/q$ = thermal voltage

N_c = effective density of states in the conduction band

N_d = impurity (donor) doping concentration

The open circuit voltage is given by [11]:

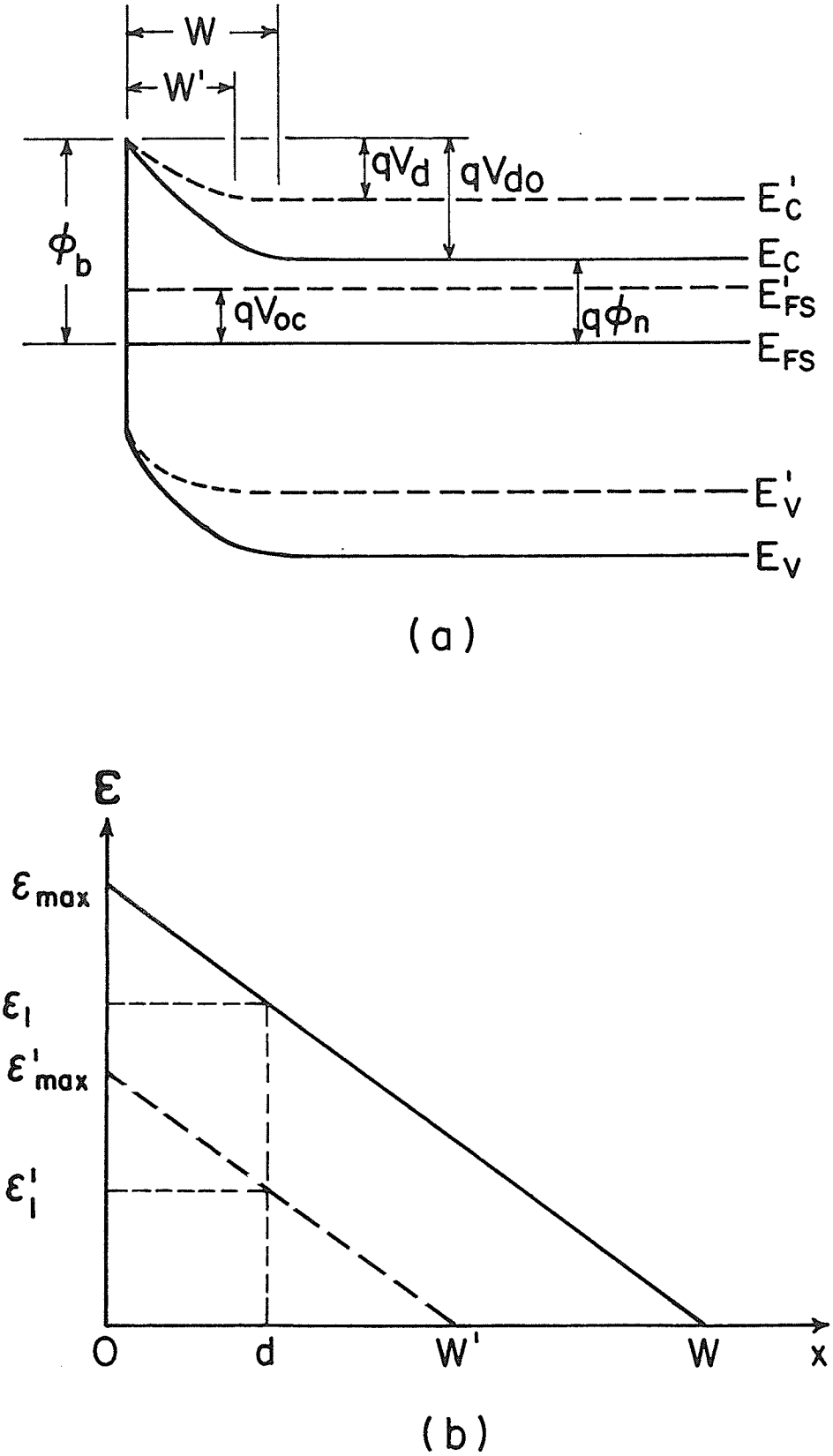

Figure 2.2: a) Energy band diagram of a metal-N-type semiconductor for dark (solid line) and illuminated (broken line) conditions ; b) Electric field distribution in the semiconductor for both dark (solid line) and illuminated (broken line) conditions

$$V_{oc} = V_T \ln \left(\frac{qF_{ph}}{J_o} + 1 \right) \qquad (2.2)$$

where

F_{ph} = the intensity of the absorbed radiation (photons/s/m^2)

J = the dark current density (A/m^2)

$= A^{**} T^2 \exp(- \phi_b/V_T)$

where

A^{**} = the modified Richardson constant ($A^{**} = 4.4$ A cm^{-2} K^{-2} [12] for n-type GaAs)

T = absolute temperature

ϕ_b = the Schottky barrier height

k = Boltzmann constant

The diffusion potential is given by [10]:

$$V_d = \phi_b - \phi_n - V_{oc} \qquad (2.3)$$

It should be noted that for the optically-illuminated case, in which the open circuit voltage (V_{oc}) is greater than

zero, the diffusion potential is reduced from its dark value, and consequently the electric field is reduced at all points in the semiconductor space-charge region.

Even though a quantitative disagreement occurs between theory and experiment for very low electric fields, at relatively high fields, the theory is quite accurate. The smallest electric field used in these calculations is orders of magnitude greater than the point at which a discrepency can be observed.

On the basis of the depletion approximation, the width of the space-charge region is given by [10]:

$$W = \left[\frac{2\,\varepsilon_o\,\varepsilon_r}{q\,N_d}\,V_D \right]^{1/2} \qquad (2.4)$$

and the maximum electric field, which occurs at the surface of the semiconductor, is given by [10]:

$$\varepsilon_{max} = \frac{q\,N_d\,W}{\varepsilon_o\,\varepsilon_r} = \left[\frac{2q\,N_d}{\varepsilon_o\,\varepsilon_r}(\phi_b - \phi_n - V_{oc}) \right]^{1/2} \qquad (2.5)$$

where

ε_o = permittivity of free space

ε_r = relative permittivity of GaAs

and the electric field distribution is given for $0 < x < W$ by [10]

$$\varepsilon(x) = \varepsilon_{max}(1 - \frac{x}{W}) \tag{2.6}$$

where x is the distance from the metal contact.

Fig. 2.3 shows the geometry of the Schottky barrier device under consideration. This device is free of any electrical connections to the metal or semiconductor, and is therefore in the open-circuit condition. It is assumed that the electric field changes only in the x direction and is constant in the y direction. This is appropriate provided the intensity of the absorbed radiation in the (controlled) beam 2 is much smaller than that in the (controlling) beam 1.

Figure 2.4 shows the absorption coefficient of GaAs as a function of photon energy for several values of electric field. The optical absorption coefficient of beam 2 is determined by the electric field and it is therefore also independent of y. Note that unlike the optical signal of beam 2 the illumination of beam 1 is entirely absorbed by the sample. This is because the photon energy for beam 1 is well in excess of the energy gap, with a very large absorption coefficient, independent of the electric field. In all cases, beam 1 is absorbed in the surface region of the ma-

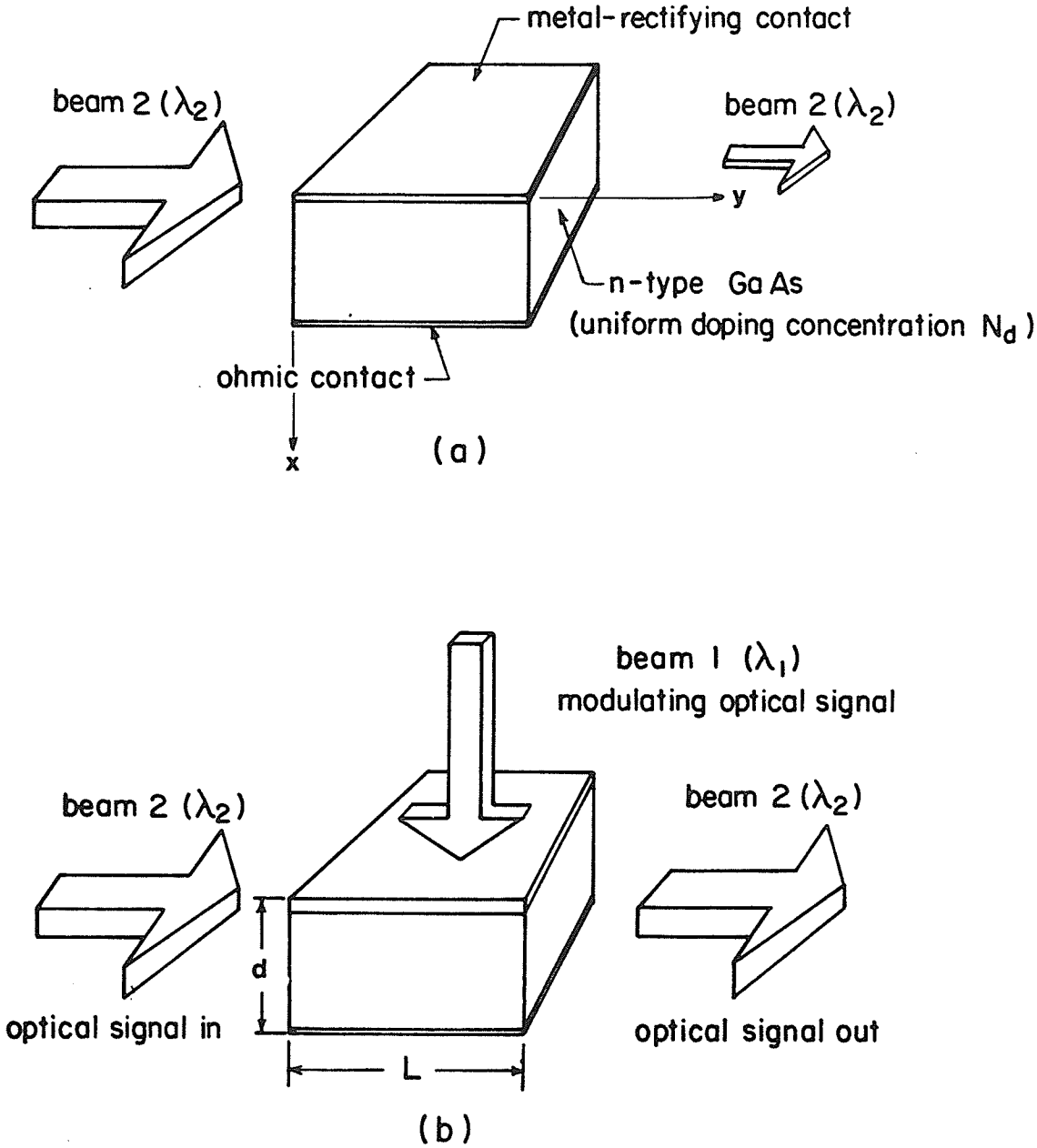

Figure 2.3: Geometry of semiconductor opto-optic modulator

terial but by the photovoltaic effect, this affects the electric field throughout the space-charge region.

The intensity of the optical signal in beam 2 at any point is given by [9]:

$$I(x,y) = I_o \exp(-\alpha(x)y) \tag{2.7}$$

where

I_o = the intensity of the signal at y=0 (ignoring reflection at the surface)

α = the absorption coefficient

y = distance along axis of propagation of beam 2

By integrating over x we obtain the total intensity in beam 2 for a given value of y. This is given by

$$I(y) = \frac{I_o}{d} \int_o^d \exp(-\alpha(x)y)\, dx \tag{2.8}$$

where

d = aperture of sample (to beam 2) in x direction

If the doping concentration of the sample is sufficiently low, the width of the space-charge region (W) as given by

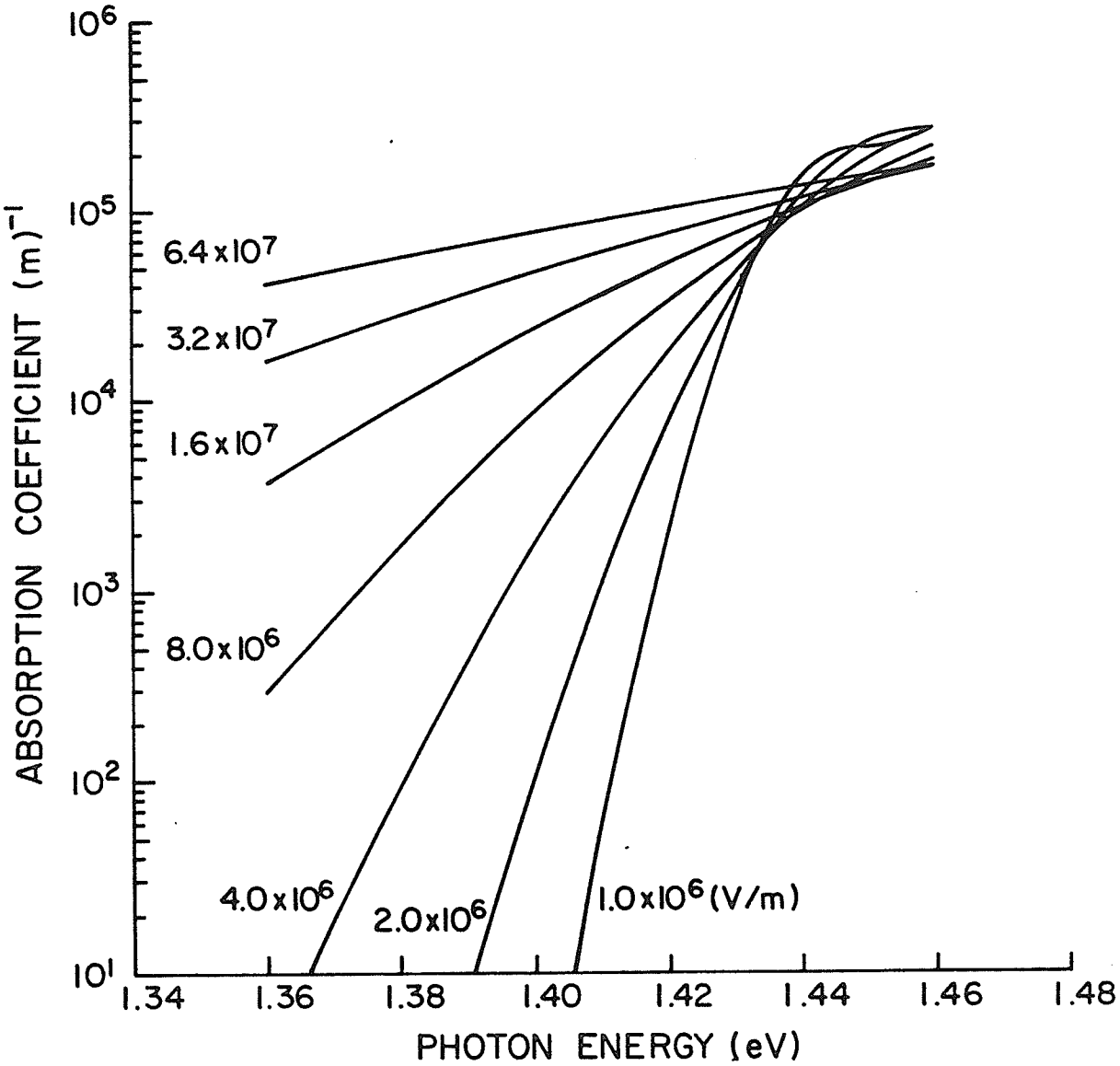

Figure 2.4: Absorption coeficient versus photon energy for several values of electric field.

Eqn.(1.4) is relatively large. Under these conditions, W can considerably exceed d while the size of this aperture remains sufficiently large to avoid serious diffraction effects to beam 2. These diffraction effects will become problematic at small aperatures ($d \sim \lambda$). One expects a variation of the output intensity of beam 2 in the x direction from 0 to d. This is due to the change with x in the electric field and consequently the optical absorption coefficient. To minimize this effect one should attempt to make the aperture (d) of the device somewhat smaller than the width (W) of the space-charge region. Using Eqns (2.5) through (2.8), the overall transmission (or normalized intensity) of beam 2 emerging at L can be written as

$$T = \frac{I(L)}{I_o} = \frac{1}{\varepsilon_{max} - \varepsilon_1} \int_{\varepsilon_1}^{\varepsilon_{max}} \exp(-\alpha(\varepsilon)y)\, d\varepsilon \qquad (2.9)$$

where ε_{max} is given by Eqn. (2.4) as a function of W (i.e. of V_{oc}). and where

$$\varepsilon_1 = \varepsilon_{max} \left(1 - \frac{d}{W}\right) \qquad (2.10)$$

The calculation of the absorption coefficient was carried out according to the model of Calloway [4,5]. The absorption coeffiecient for a GaAs sample is given by :

$$\alpha = \frac{2\pi}{\omega} k\beta^{1/2} \mu \left[\left(\frac{dA_i(y)}{dy} \right)^2 \Bigg|_{y_o} - y_o (A_i(y_o))^2 \right] \tag{2.11}$$

where

$$k = \frac{2\, e^2 |\bar{e} \cdot \bar{P}_{nn'}|^2}{\pi\, \hbar^2\, m^2\, n\, \varepsilon_o\, C} \tag{2.12}$$

$$\beta = \frac{2\mu\, \varepsilon}{\hbar^2} \tag{2.13}$$

$$y_o = \frac{2\mu}{\hbar^2\, \beta^{2/3}} (E_{gap} - \hbar\omega) \tag{2.14}$$

$$\frac{1}{\mu} = \frac{1}{m_e^*} + \frac{1}{m_h^*} \tag{2.15}$$

and where

ω = the frequency of optical radiation

ε = the electric field

$\hbar$ = Planck constant

$\overline{P}_{nn'}$ = the interband momentum matrix element

$\overline{e}$ = the polarization vector of the radiation

m_e^* = the effective mass of electrons

m_h^* = the effective mass of holes

n = the index of refraction

ε_o = the permittivity of free space

m_o = the free electron mass

E_{gap} = the energy gap (eV)

c = the velocity of light

$Ai(y)$ = the Airy integral

The Airy integral is given by [9]:

$$A_i(y) = \int_0^\infty \cos(sy + \frac{s^3}{3})\, ds \tag{2.16}$$

and the power series representation of this integral by [9]

$$A_i(y) = C_1\, f(y) - C_2\, g(y) \tag{2.17}$$

where

$$f(y) = 1 + \frac{1}{3!} y^3 + \frac{1.4}{6!} y^6 + \frac{1.4.7}{9!} y^9 + \ldots \tag{2.18}$$

$$g(y) = y + \frac{2}{4!} y^4 + \frac{2.5}{7!} y^7 + \frac{2.5.8}{10!} y^{10} + \ldots \tag{2.19}$$

$$C_1 = A_i(0) = \frac{3^{-2/3}}{\Gamma(2/3)} \tag{2.20}$$

$$C_2 = A_i'(0) = \frac{3^{-1/3}}{\Gamma(1/3)} \tag{2.21}$$

For small electric fields which correspond to large arguments of the Airy integral, the following approximations have been adopted [5].

$$A_i(y) \simeq \frac{1}{2} \pi^{1/2} y^{1/4} \exp(-\frac{2}{3} y^{3/2}) \tag{2.22}$$

$$A_i(-y) = \pi^{-1/2}\, y^{-1/4} \sin(\frac{2}{3} y^{3/2} + \frac{\pi}{4}) \qquad (2.23)$$

The transmission (or normalized intensity) for both optically illuminated (by beam 1) and non-illuminated cases were calculated as functions of the doping concentration (N_d), of the photon energy ($\hbar\omega_2$) of the controlled optical signal (beam 2) and of the length (L) of the sample (in the y direction). The difference in the transmission between the two cases was also calculated as a function of the these parameters. For the purposes of calculation an algorithm based upon Simpson's Rule for numerical integration was employed (see Appendix "B" for program listing). Double precission was adopted to ensure the desired accuracy. This program was run on the Amdahl V7 mainframe computer at the University of Manitoba.

2.3 RESULTS

In this section, we present results of calculations of the optical absorption of beam 2 and of its transmission through the GaAs Schottky barrier device. These calculations are dependent upon the physical characteristics of the device as well as upon those of the optical sources. Two (binary) conditions are considered. These are (1) the modulating

(control) signal, beam 1, is not present, (the 'off' case), and (2) the control signal beam 1 is present and is totally absorbed by the semiconductor device, (the 'on' case). For the off case, the electric field distribution corresponds to that of a dark Schottky barrier as given in Eqns. (2.4) to (2.7) with $V_{oc} = 0$. This electric field distribution determines the absorption coefficient of beam 2 which has a photon energy close to the energy gap of GaAs. The transmission of beam 2 is intended in this case to be very small, most of it being absorbed before reaching y = L in Fig. 2.2 . For the on case an open-circuit voltage (V_{oc}) is induced by the absorption of beam 1, which greatly reduces the electric field at all points in the path of beam 2, by reducing ε_{max} in Eqn. (2.5) and hence $\alpha(x)$ in Eqn. (2.7) Under these conditions in which the absorption coefficient is reduced, the sample becomes relatively transparent to beam 2. The intensity of beam 1, is in the on case, of an appropriate magnitude (5×10^{20} photons/cm^2/s ; 8 milliwatts/cm^2) to induce an open-circuit voltage V_{oc} = 0.6 (V) in the GaAs device acoording to Eqn. (2.2). It should be noted that, unlike beam 2, the control beam need not be monochromatic in order to develop the photovoltaic effect. The intensity required here is easily obtainable from reasonable broad band sources. We have chosen a diffusion potential of $V_d = 0.95$ V for dark conditions ($V_{oc} = 0$) which is typical of a Au-GaAs Schottky barrier [10]. Note

that the metal (in this case a thin film of Au) is sufficiently thin to be transparent to beam 1. Its thickness should be < 100 Å according to expermental work on Schottky barrier solar cells [14]. The employment of the metal film is not strictly requried, as a free surface also develops a photovoltage provided it is depleted as a consequence of surface states. Use of the metal is expected, however, to stabilize the (dark) diffusion potential, and improve reliability.

In figure 2.5, the dependence of the transmission is shown for the 'off' (T_{off}) case upon photon energy ($\hbar\omega_2$), for several values of doping concentration (N_d). Fig. 2.6 shows results of similar calculations for the 'on' case (T_{on}).

The dependence of the T_{off} upon photon energy for several values of sample length L is shown in Fig 2.7 The corresponding results for T_{on} are shown in figure 2.8

Figures 2.9 a), b) and c) show contour plots for the difference (T_{on} - T_{off}) in the transmission of beam 2 for the two cases. This is a measure of the discrimination of the device between the two states. The dependence of this difference upon photon energy ($\hbar\omega_2$), doping concentration (N_d) and the sample length (L) is illustrated.

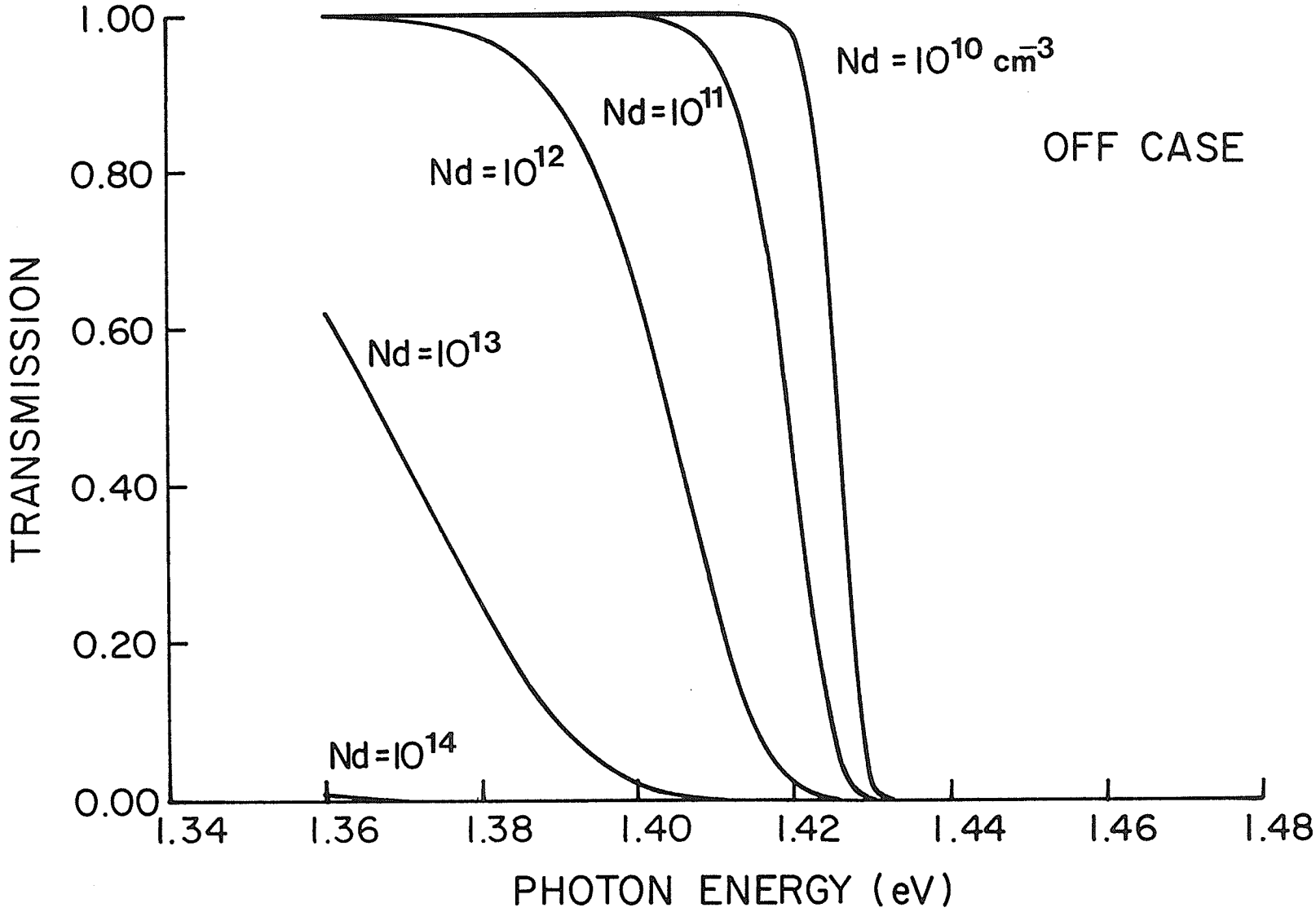

Figure 2.5: Transmission (T_{off}) vs photon energy for several values of doping concentration (N_d) for the non-illuminated (by beam 1) case, L = 10-4 m

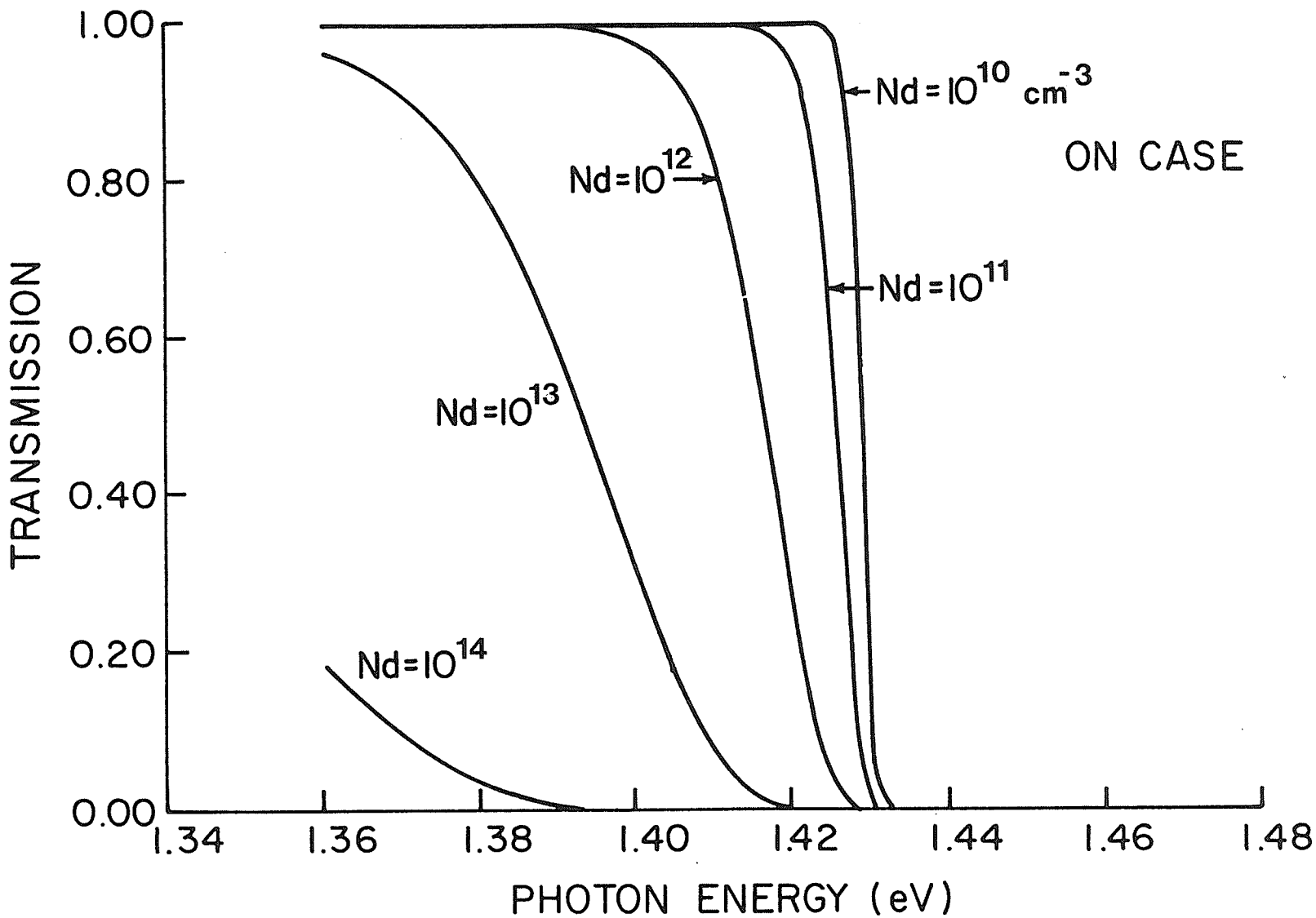

Figure 2.6: Transmission (T_{on}) vs photon energy for several values of doping concentration (N_d) for the illuminated (by beam 1) case, L = 10^{-4} m

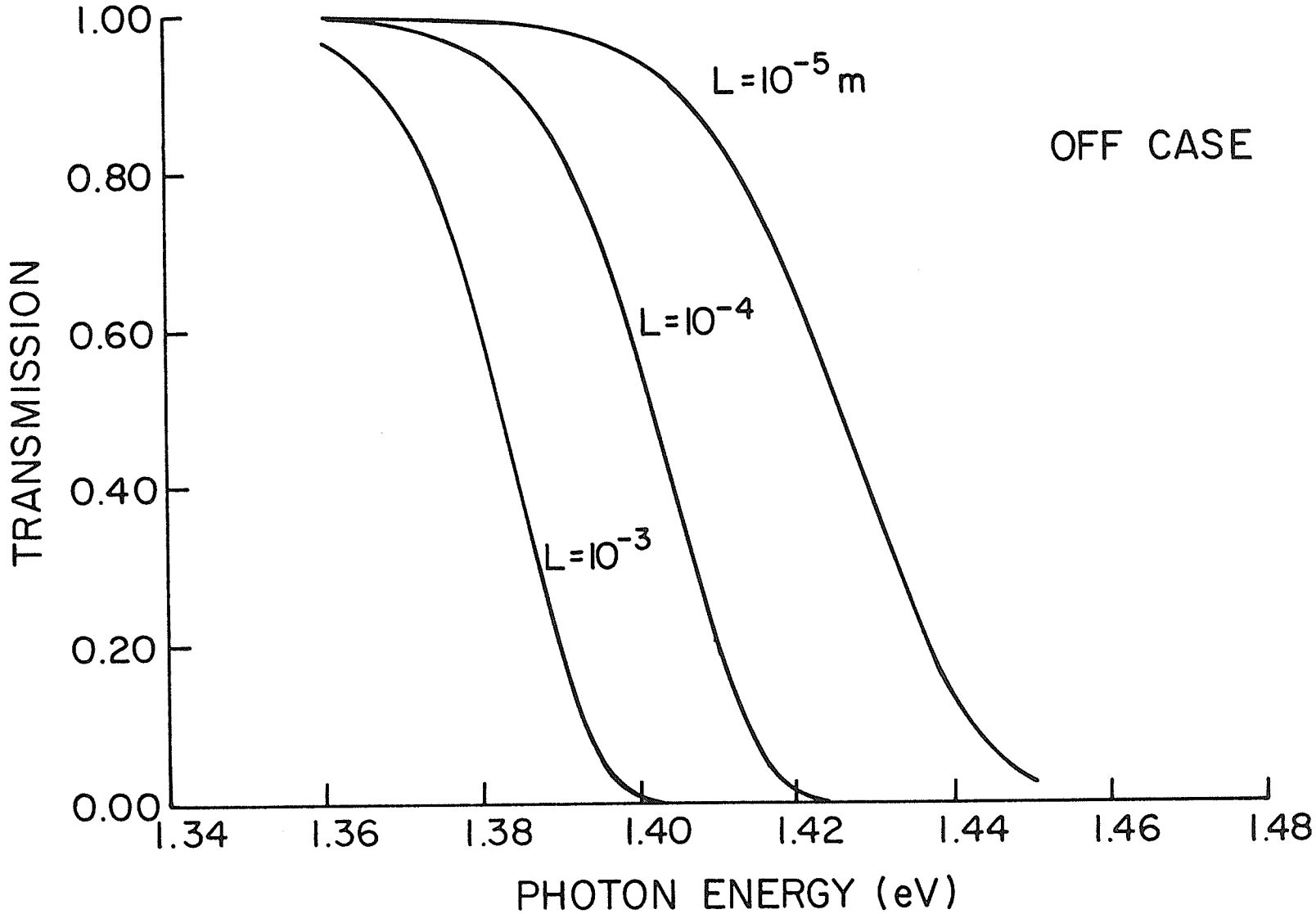

Figure 2.7: Transmission (T_{off}) vs photon energy for several values of sample length (L) for the non-illuminated case, $N_d = 10^{12}$ cm^{-3}

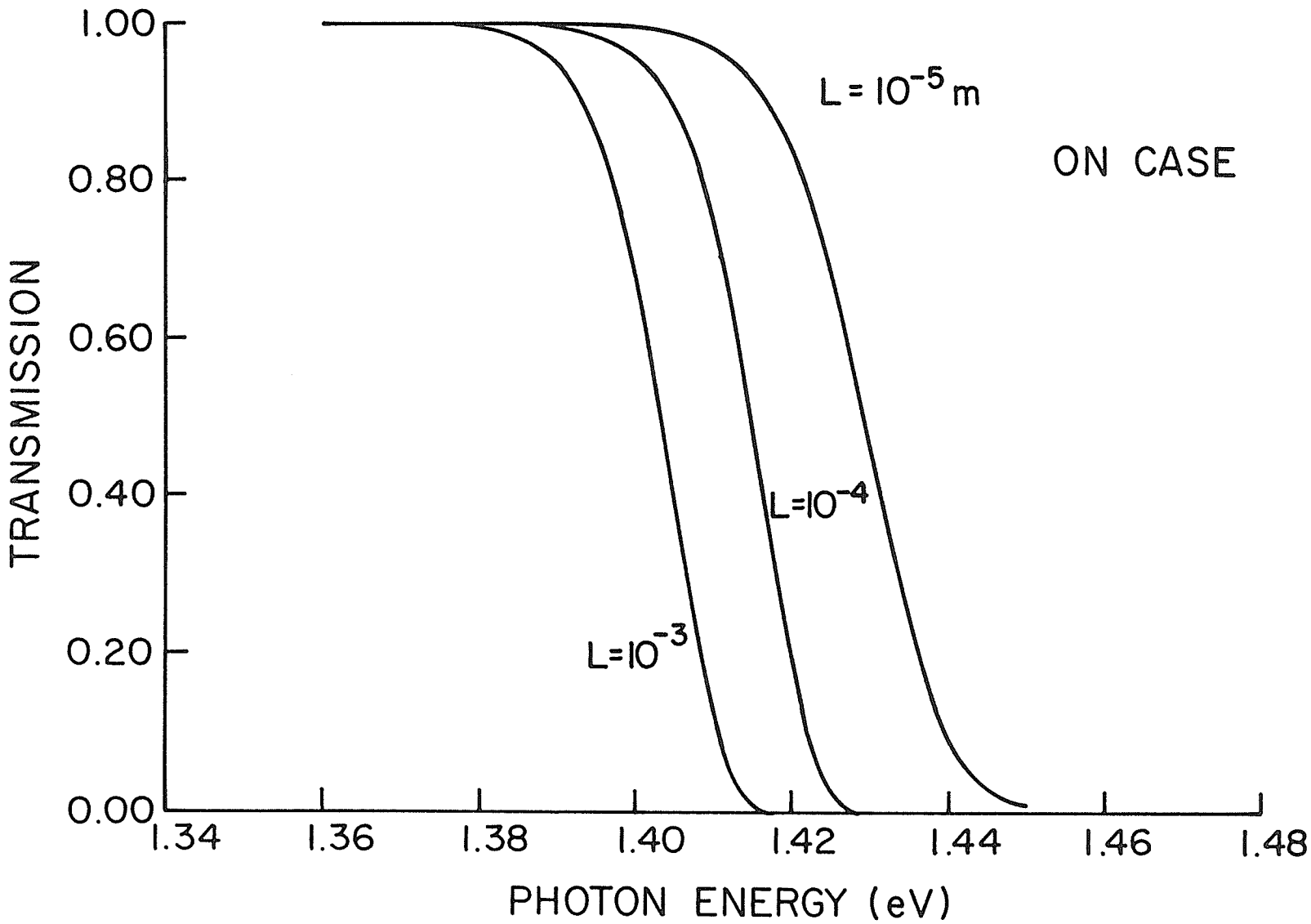

Figure 2.8: Transmission (T_{on}) vs photon energy for several values of sample length (L), for the illuminated case (by beam 1) case, $N_d = 10^{12}$ cm^{-3}

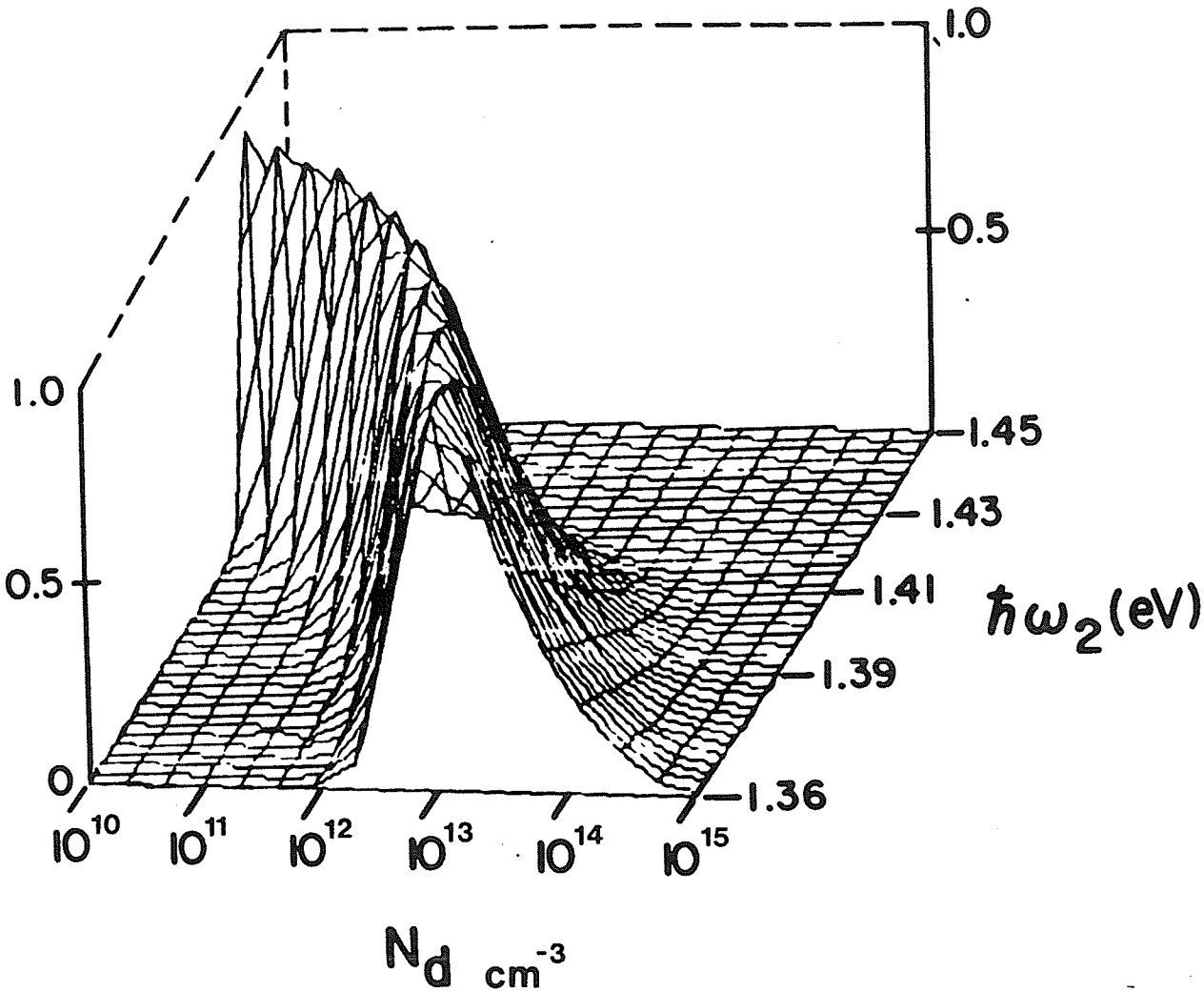

Figure 2.9: a) Three dimensional contour plot of transmission discrimination ($T_{on} - T_{off}$) versus photon energy and doping concentration, $L = 10^{-3}$ m.

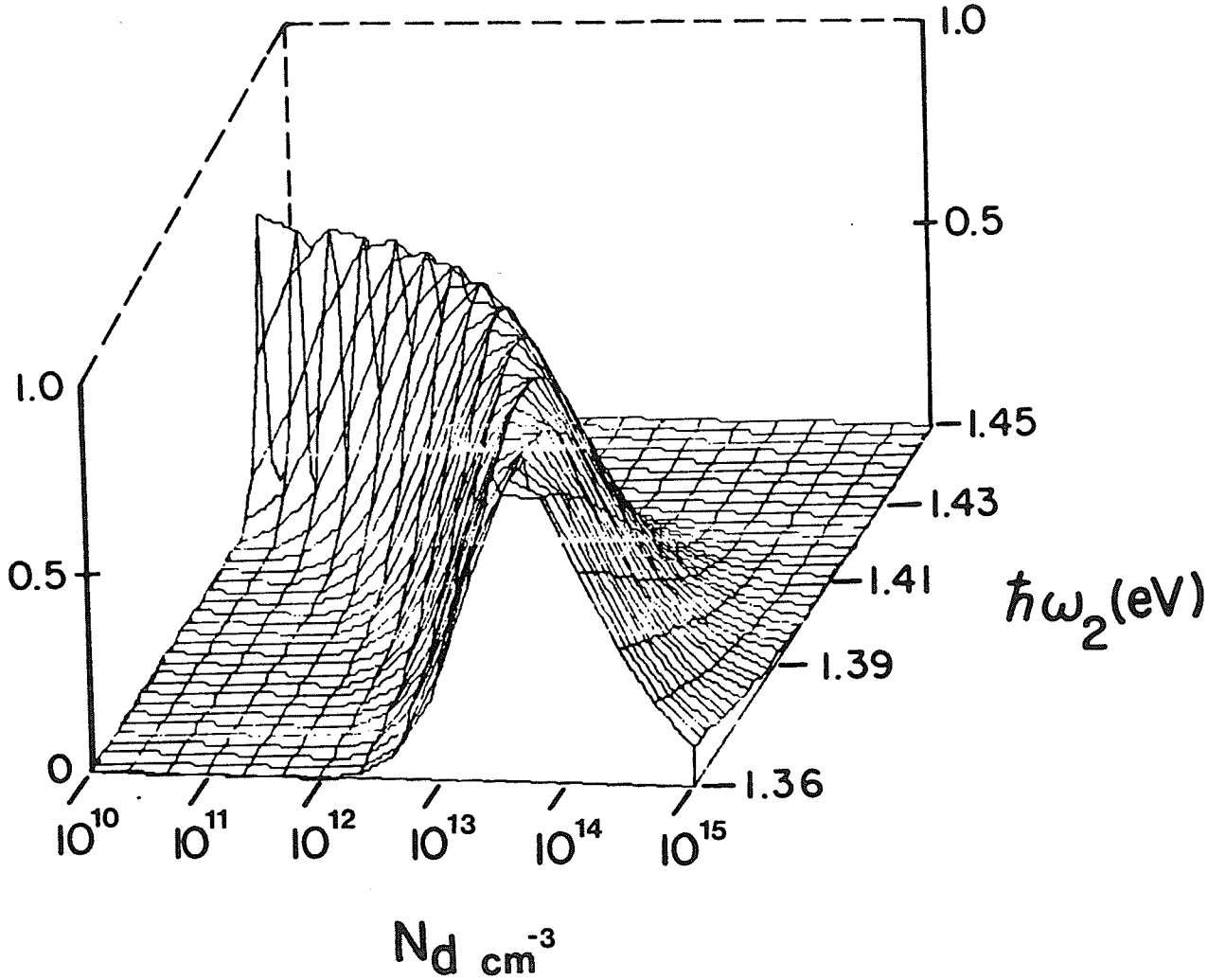

Figure 2.9: b) L = 10^{-4} m .

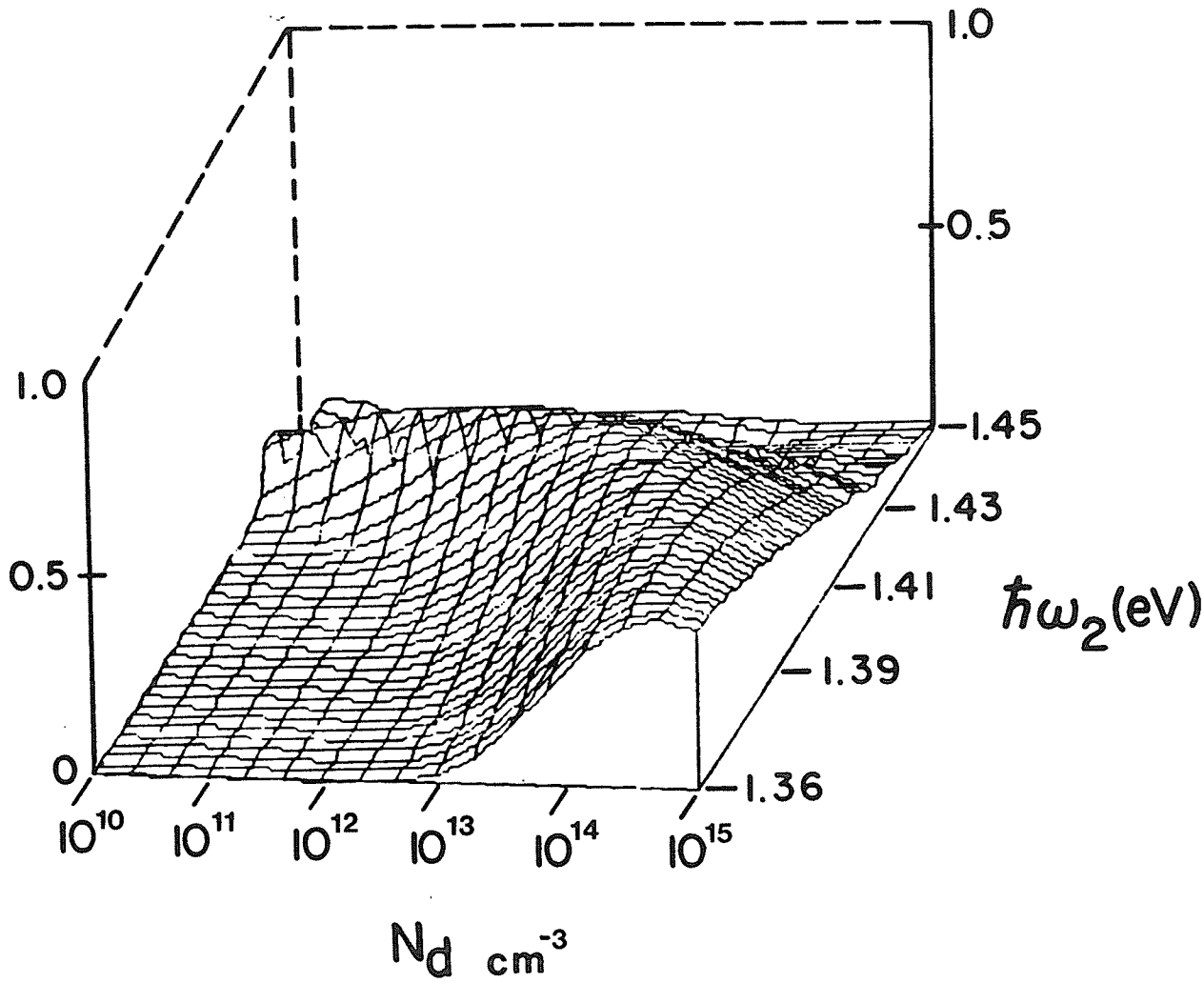

Figure 2.9: c) L = 10^{-5} m .

2.4 DISCUSSION AND APPLICATIONS

From Fig. 2.4, we confirm that in accordance with the Franz-Keldysh effect, the optical absorption of GaAs for photon energies in the neighborhood of the energy gap shows a strong dependence on the electric field in the material. Below the energy gap a doubling of the electric field can produce a change in the optical absorption by one or more orders of magnitude. Therefore by manipulating the internal electric field in the space-charge region of a GaAs device the optical absorption can be effectively modulated. As the photon energy increases above that of the energy gap E_{gap}, Fig. 2.4 shows that the absorption varies only slightly with the electric field in comparison with photon energies below the gap. The electric field in the space-charge region can be effectively adjusted by means of the photovoltaic effect. Using a modulating signal (beam 1) with photon energy well in excess of E_{gap} we can therefore adjust the field and effectively modulate absorption of the transmitted signal (beam 2) with photon energy just below E_{gap}. This change in absorption can be adjusted to produce almost total transparency or total absorption of the propagating signal.

In general from Figs. 2.5 through 2.8, we show that as the photon energy of the transmitted signal (beam 2) approaches the energy gap the transmission of this signal goes to zero. For very low doping concentrations ($N_d < 10^{10}$ cm^{-3}), the transition with photon energy in the

transmission from 100% to 0% is very abrupt for both on and off cases of the controlling signal (beam 1). This change occurs very close to the energy gap. Referring to Fig. 2.4 and Eqn. (2.5) we see that the relatively low electric field associated with the low doping concentrations (Eqn. (2.5)) are responsible for this behaviour. For larger doping concentration (N_d) and hence higher electric fields these transitions with photon energy from total absorption to total transparency are much less abrupt. For values of $N_d > 10^{14}$ cm^{-3}, the absorption of beam 2 is so great that we can consider the device totally opaque in both 'on' and 'off' cases, for photon energies within the vicinity of the gap. This is shown in Figs. 2.5 through 2.8 Also for photon energies above the gap, Fig. 2.4 shows that the absorption (of beam 2) will be very high and thus the transmission very low in all cases. This is inherent from the the band structure of the device and is relatively independent of the doping concentration. The lower limit for the doping concentration (for maximum transmission of beam 2) is the intrinsic carrier concentration. Oxygen-doped, compensated [15] and undoped [15a] GaAs samples have been produced with close to intrinsic carrier concentrations. The intrinsic carrier concentration for GaAs is $n_i \approx 10^6$ cm^{-3}. The range of dopings that give reasonable transmission in the 'on' case are from $N_d = n_i$ to $N_d = 10^{13}$ cm^{-3} with optimum N_d dependent upon .

From Eqn (2.9) we see that the transmission is exponetially depenedent on the length (L) of the device. An increase in the length (L) will rapidly decrease the transmission of beam 2. For $L < 10^{-5}$ m, the device appears almost transparent for photon energies of beam 2 below the energy gap. As the length of the sample increases ($L > 10^{-3}$ m), the transmission of beam 2 for energies close to the gap, becomes very low. This behavior can be observed in Figs. 2.6 and 2.7 .

In order to consider applications of this device in digital (binary) signal processing, $T_{on} - T_{off}$ must be maximized. For any photon energy less than the energy gap, the transmission of beam 2 is always greater for the on case (beam 1) than the off case. This holds for all values of doping concentration (N_d) and sample length (L) considered. For very low doping concentrations ($N_d < 10^{10} cm^{-3}$), $T_{on} - T_{off}$ approaches unity (100%) at a photon energy $\hbar\omega_2 = E_{gap}$. From Fig. 2.9 (a) we can see that for large doping concentrations ($N_d > 10^{14} cm^{-3}$) and/or for photon energies well above the gap, $T_{on} - T_{off}$ approaches zero. In this case, the electric field (given by Eqn. (2.5)) is so high that for both on and off conditions the respective transmissions are near zero. Their difference therefore is also near zero. This corresponds to the sample being unconditionally opaque. On the other hand the GaAs sample becomes almost totally transparent for the condition where the

doping concentration is very small ($N_d < 10^{10}$ cm^{-3}) ; for this case $T_{on} = T_{off} = 1$ and once more their difference is zero. In this situation the sample is uncoditionally transparent. The maximum discrimination occurs at doping concentrations $10^{12} < N_d < 10^{14}$ cm and for photon energies $h\omega_2$ well below E_{gap}. For energies nearer E_{gap}, the maximum discrimination occurs at much lower doping concentrations $N_d < 10^{10}$ cm^{-3}.

For maximum discrimination $\hbar\omega_2 \simeq E_{gap}$ and $N_d < 10^{10}$ cm^{-3}, in which case both T_{on} and T_{off} experience sharp transitions from 100% transmission to 0% transmission. Each respective transition occurs at a different photon energy (see Figs. 2.5 and 2.6 or Figs. 2.7 and 2.8). From these figures we can see there is an optimum range of photon energy where the transmission $T_{on} = 1$ and $T_{off} = 0$; ($1.42 < \hbar\omega_2 < 1.44$ eV). This correnspondsto a 1-2 % change in the photon energy or wavelength and imposes a requirement for a highly monochromatic (i.e. single mode) laser source for beam 2. A GaAs laser emits at approximately 904 nm which corresponds to a photon energy Eph = 1.37 eV. With a small molar fraction of aluminum (x) in a $Al_x Ga_{1-x}$ As laser, one can reduce the central wavelength of the laser source below $\lambda \simeq 0.904$ µm , decreasing with x to $\lambda = 0.845$ µm at x = 0.08 [15,16]).

Due to the small physical aperture (d) of the device imposed by the narrow space-charge region, diffraction effects

on beam 2 should also be considered. For a uniform output intensity of beam 2, d must be less than the width of the space-charge region (W) given by Eqn (2.4). For the device under consideration in this thesis we have employed an aperture width $d = W'/2$ where W' is the width of the space-charge region under illumination (given by Eqn (2.4)). The diffusion potential (V_d), including the open-circuit voltage was $V_{oc} = 0.2$ V. To eliminate the diffraction of beam 2, the width $W'=2d$ should then be much greater than the wavelength (λ) [18].

Specifically we will consider a laser source (beam 2) as having a wavelength $\lambda = 0.870$ μm. This wavelength (λ) corresponds to a Al_xGa_{1-x} As semiconductor laser with x = 0.04. This corresponds to a photon energy of $\hbar\omega_2 = 1.43$ eV, that of the energy gap of GaAs at 300 K. For $N_d = 10^{10}$ cm^{-3} , $W' = 1.10 \times 10^{-4}$ cm so that $d = W'/2 \gg \lambda$, the diffraction effects for beam 1 become small. For larger doping the width of the space-charge region is decreased according to Eqn (2.4) until $N_d \simeq 10^{14}$ cm^{-3} , where $W \simeq \lambda$ and diffraction effects would have to be considered.

As discussed above the operation of the device under consideration is very sensitive to changes in the wavelength of the transmitted signal. Figures 2.9 (a), 2.9 (b) and 2.9 (c) all show the dependence of the discrimination (T_{on} - T_{off}) upon photon energy. For a typical semiconductor las-

er, the spectral width is usually on the order of a few angstroms [19]. This will correspond to a spectral width on the order of 0.1 % of λ . Recent advances in the single mode $Al_x Ga_{1-x} As$ lasers have reduced the spectral width to $\Delta\lambda < 1$ Å [for example 15,16,20] . The spectral width of the laser in these cases is much smaller than the range of photon energy for maximum discrimination in Fig. 2.9 (a).

New advances in integrated optics have created the need for optical devices that can be incorporated into integrated optical systems. The opto-optic modulator proposed in this thesis can perform digital optical logic for these applications. Analog operation of this device was not discussed in this thesis, but it is clear that analog aplications are also possible.

Chapter III

PHOTON COUNTING STATISTICS ASSOCIATED WITH TEMPERATURE FLUCTUATIONS IN SEMICONDUCTOR LASERS *

3.1 INTRODUCTION

Statistical photon counting distributions for coherent sources of radiation have been discussed by many authors [see for example Refs 22-25]. However in their determination of these distributions, these studies usually considered sources either with constant amplitudes or with specific types of modulation (i.e. pulsed, triangular, sine wave [25]). In this paper, on the other hand, the modulation is in the form of a stationary random process.

Since the advent of the laser, and specifically of the semiconductor laser, the development of the photon/photoelectron counting distributions and of the experimental determination of these distributions have been of great interest. Intrinsic fluctuations of the output intensity of semicondutor lasers have been dealt with by Paoli [26,27]. These intensity fluctuations are usually attributed to noise in the lasers. Modal, shot noise and noise due to spontane-

---

* The contents of this chapter have been submitted for publication [21].

ous emission in the laser can all account for stochastic fluctuations in the output intensity. Fluctuations in the operating temperature of the device will also give rise to intensity fluctuations [28,29]. Given that the temperature of a certain environmental condition is stochastic, then the intensity fluctuations due solely to changes in the temperature will be stochastic. The photon counting statistics associated with temperature fluctuations in semiconductor lasers is the subject of this investigation.

3.2 THEORY

We consider first a monochromatic source that is illuminating an ideal detector, whose internal quantum efficiency is unity. Since the nature of the source is being explored, we assume the area of the detector is much smaller than the coherence area of the source. The detected photons will have a statistical distribution about a mean value with a characteristic coherence time. This is simply due to the statistical nature of the arrival rate of the photons. There will then be a particular probability associated with the detection of n photons within a certain time interval T. This distribution is given by the Mandel formula (simple Poisson statistics) in the absence of intensity fuctuations (i.e. constant mean value) [24]

$$p(n|\lambda_o) = \frac{\lambda_o^{-n} e^{-\lambda_o}}{n!} \tag{3.1}$$

where

λ_o = < n > is the time average of the distribution over the interval T (i.e. the average intensity)

$$\lambda_o = \int_t^{t+T} I(t')\, dt' \qquad (3.2)$$

and where

I = the intensity of the laser

Now consider the situation where the time-averaged value (λ_o) is not constant over the time interval of interest (T). We assume here that the time-averaged value is described by a stochastic process. This could be analogous to the random intensity fluctuations that are inherent in semiconductor lasers.

It has been found [28] that the output intensity (I) and subsequently the time averaged intensity (λ) of a semiconductor laser (well above theshold) vary linearly with the laser diode current density (J). We have

$$\lambda = k_1 J \qquad (3.3)$$

where

k = a constant of proportionality

λ = time averaged laser intensity

J = laser diode current density

The threshold current of the source varies exponentially with temperature [29].

$$J_{th} = k_2 \exp\left(\frac{T}{T_o}\right) \tag{3.4}$$

where

J_{th} = threshold current density of the laser

k = is a constant of proportionality

T = is the temperature

T_o = is a constant dependent upon the laser type

Over a wide range of temperatures the variation in threshold current due to the fluctuations in temperature will produce a corresponding change in the operating current of the source. The relationship between the variation in threshold current and the operating current was assumed to be linear

over the range of interest. From the data of Tsang et al [30], for GaAs - $Al_x Ga_{1-x}$ As buried stripe lasers, the range of operating temperatures that would produce this linear variational relationship was found to be 25 ^oC to 100 ^oC. Therefore within this range, the operating current and subsequently the output intensity of the laser will vary exponentially with temperature. By letting $J = k_3 J_{th}$ and by substituting Eqn. 3.4 into Eqn. 3.3 we obtain

$$\lambda = k \exp \left(\frac{T}{T_o} \right) \tag{3.5}$$

where

λ = time averaged laser intensity

T = temperature

k = a constant of proportionality

The value of the parameter T_o plays an important role in the final determination of the photon distribution. It describes the temperature sensitivity of the laser source [31]. The currently available literature offers no concise theory of its origin. It is dependent on a number of variables that makes its theoretical determination almost impossible. Therefore a phenomenological/experimental approach has been taken.

Experimentally the value of T_o has been found to be 60 - 70 K for T > 250 K and 110 K for T < 250 K for InGaAsP - InP double-heterostructure (DH) lasers [32,38]. For GaAs - $Al_x Ga_{1-x}As$ DH lasers T ≃ 150 - 180 K for the temperature range 100 K < T < 350 K [32,36]. The value of T_o in this paper was chosen to be within the experimental range.

If a Gaussian probability density function $p_T(t)$ is assumed, as defined by the following relation [39]

$$
\begin{aligned}
p_T(t) &= 0 && t < 0 \\
&= \frac{1}{2}\,\mathrm{erfc}\left(\frac{t_o}{\sqrt{2}\,\sigma}\right)\delta(t) && t = 0 \qquad (3.6) \\
&= \frac{1}{\sqrt{2\pi}\,\sigma}\exp\left[-\frac{(t - t_o)^2}{2\sigma^2}\right] && t > 0
\end{aligned}
$$

where

σ = the standard deviation of temperature fluctuations (K)

t = mean temperature or operating heat sink temperature (K)

δ (t) = Dirac delta function

The probability density function of the output intensity $p_I(\lambda)$ will then be given by

$$
\begin{aligned}
p_I(\lambda) &= 0 && \lambda < k \\
&= \frac{T_o}{2K} \operatorname{erfc}\left(\frac{t_o}{\sqrt{2}\,\sigma}\right) \delta(\lambda - k) && \lambda = k \qquad (3.7) \\
&= \frac{T_o}{\sqrt{2\pi}\,\sigma} \frac{1}{\lambda} \exp\left[-\frac{(T_o \ln(\frac{\lambda}{K} - t_o))^2}{2\sigma^2}\right] && \lambda > k
\end{aligned}
$$

where

$\delta(\lambda-k)$ = the Dirac delta function

Note that the expected value of λ is

$$
\bar{\lambda} = \lambda_o = E[\lambda] = \int_{-\infty}^{\infty} \lambda\, P_I(\lambda)\, d\lambda \qquad (3.8)
$$

$$
= k \exp\left(\frac{t_o}{T_o}\right)
$$

and the constant of proportionality (k) becomes

$$k = \lambda_o / \exp\left(\frac{t_o}{T_o}\right) \tag{3.9}$$

Now Eqn. (3.7) may be rewritten in the following form.

$$p_I(\lambda) = \begin{cases} 0 & \lambda < k \\ \frac{T_o}{2\lambda_o} \exp\left(\frac{t_o}{T_o}\right) \operatorname{erfc}\left(\frac{t_o}{\sqrt{2}\,\sigma}\right) \delta(\lambda - k) & \lambda = k \\ \frac{1}{\sqrt{2}\,\sigma_1} \frac{1}{\lambda} \exp\left[-\frac{(\ln \frac{\lambda}{\lambda_o})^2}{2\sigma_1^2}\right] & \lambda > k \end{cases} \tag{3.10}$$

$\sigma_1 = \sigma / T_o$

λ = the random variable

The photoelectron probability density function is then given by

$$P_I(n) = \int_0^\infty p(n|\lambda)\, P_I(\lambda)\, d\lambda \tag{3.11}$$

This function satisfies the relation for probability distributions that

$$\int_0^\infty P_I(n)\, dn = 1 \tag{3.12}$$

Given that the probability density function of the average value of the intensity is as described above, the actual counting probability density function is be given by

$$P_I(n) \int_o^\infty \frac{\lambda^n e^{-\lambda}}{n!} \frac{1}{\sqrt{2}\,\sigma_1} \frac{1}{\lambda} \exp\left[-\frac{(\ell n \frac{\lambda}{\lambda_o})}{2\,\sigma_1^2}\right] d\lambda \qquad (3.13)$$

The calculation of this integral was performed using an algorithm based upon Simpson's rule over the interval 10^{-5} to 50.0 with a step size (h) of 0.167 (see Appendix "C" for program listing). The truncation error is of the order h for Simpson's rule.

For very small values of λ, the logarithmic singularity may be addressed by more appropriate Gauss-Quadrature schemes [40].

3.3 RESULTS AND DISCUSSION

Figures 1 through 5 show the results of the calculation of the photon distributions for four values of standard deviation of the temperature fluctuations. In each figure there are two curves. The first represents the simple Poisson distribution with a constant mean value (simple Poisson process). The second trace shows the density function that

will result from Gaussian temperature fluctuations (complex Poisson process).

Figure 3.1 shows the case for the smallest standard deviation (σ = 1). The complex Poisson distribution approaches the simple Poisson distribution as one would expect. As the standard deviation of the temperature goes to zero, the modulation function (Eqn. 3.7) approaches a Dirac delta function and the integration (Eqn. 3.13) reduces to the simple Poisson distribution (Eqn. 3.1).

The maximum standard deviation is considered in Fig. 3.5 (σ = 40). Note that the distribution broadens markedly. The mean of the density function is also shifted to a lower value. A comparison of Figs. 3.1 - 3.5 shows that as the standard deviation of the Gaussian distribution increases the downward shift of the mean also increases. It should also be noted that the density function becomes much more asymmetric with increasing temperature fluctuations.

The broadening of the curves is directly related to two parameters, T_o and σ_1 . From Eqn. 3.10, it can be seen that both the broadening and the shift depend on the value of σ_1 (for constant λ). As T_o decreases, the sensitivity of the laser to fluctuations in temperature increases. As the sensitivity increases the effect on the photon distribution will also increase for constant temperature fluctuations. Similarly if the sensitivity is constant and the size of the temperature fluctuations increases then

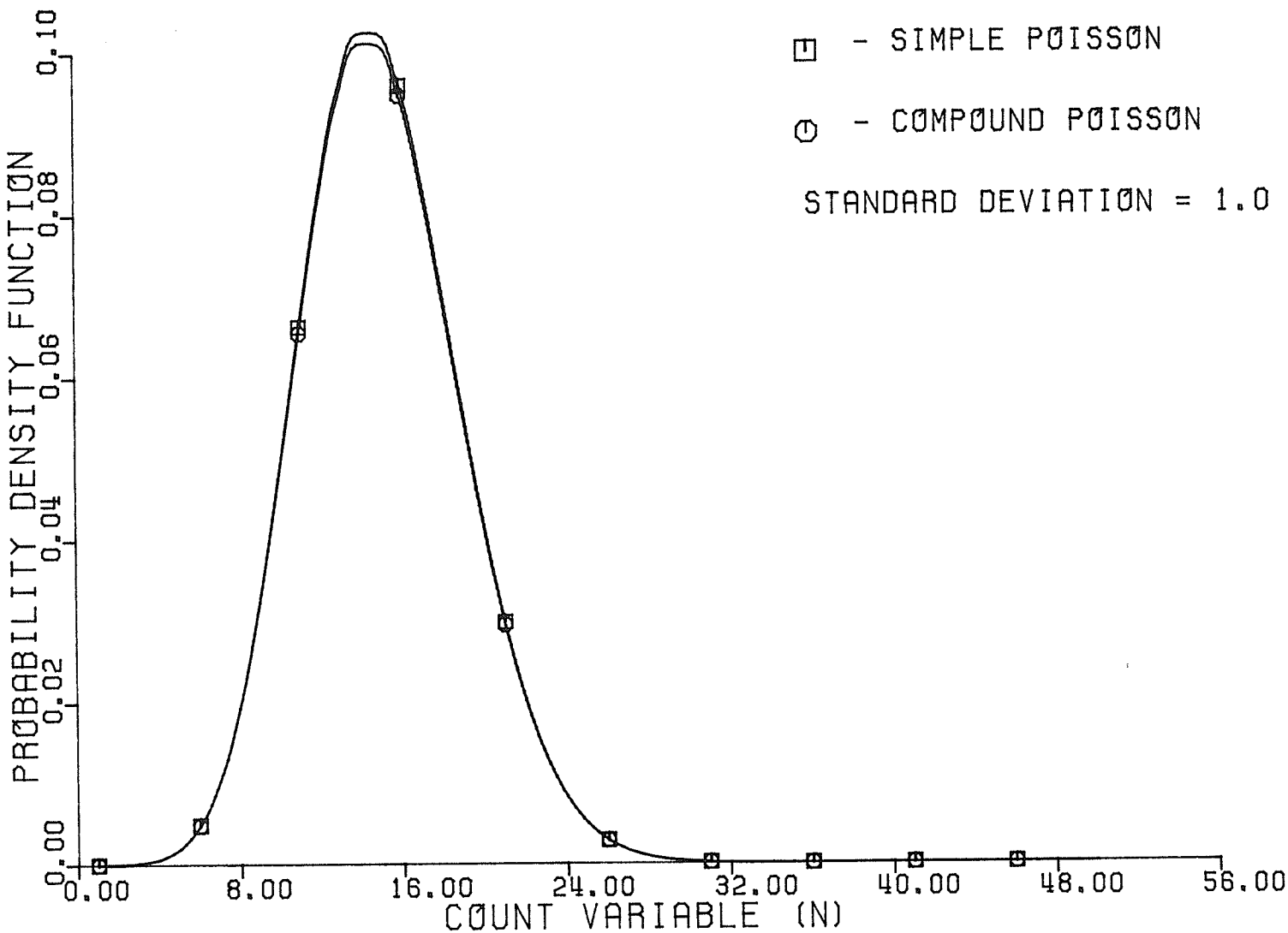

Figure 3.1: Photon probability density function,
$\sigma = 1.0$ K

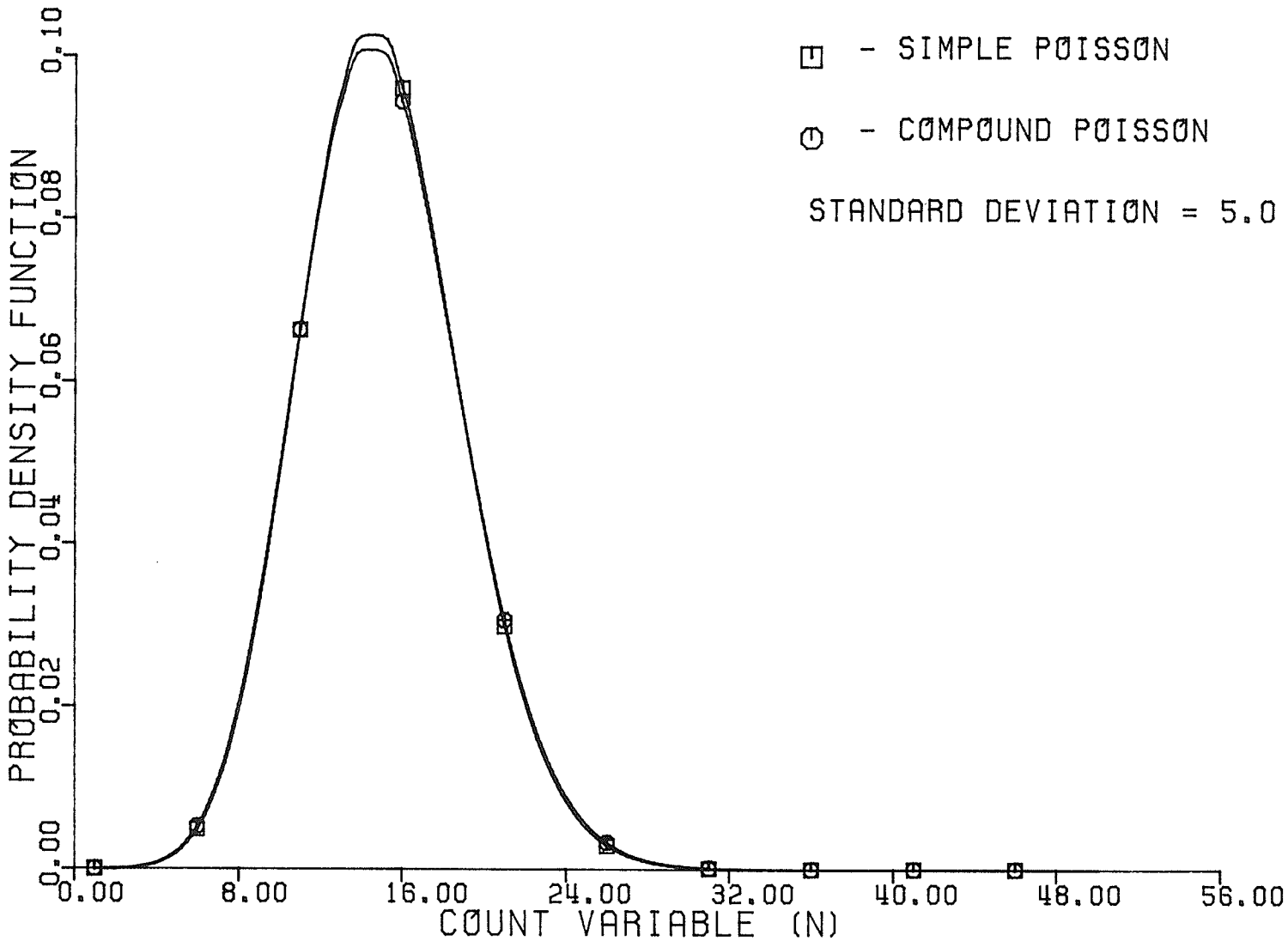

Figure 3.2: Photon probability density function, $\sigma = 5.0$ K

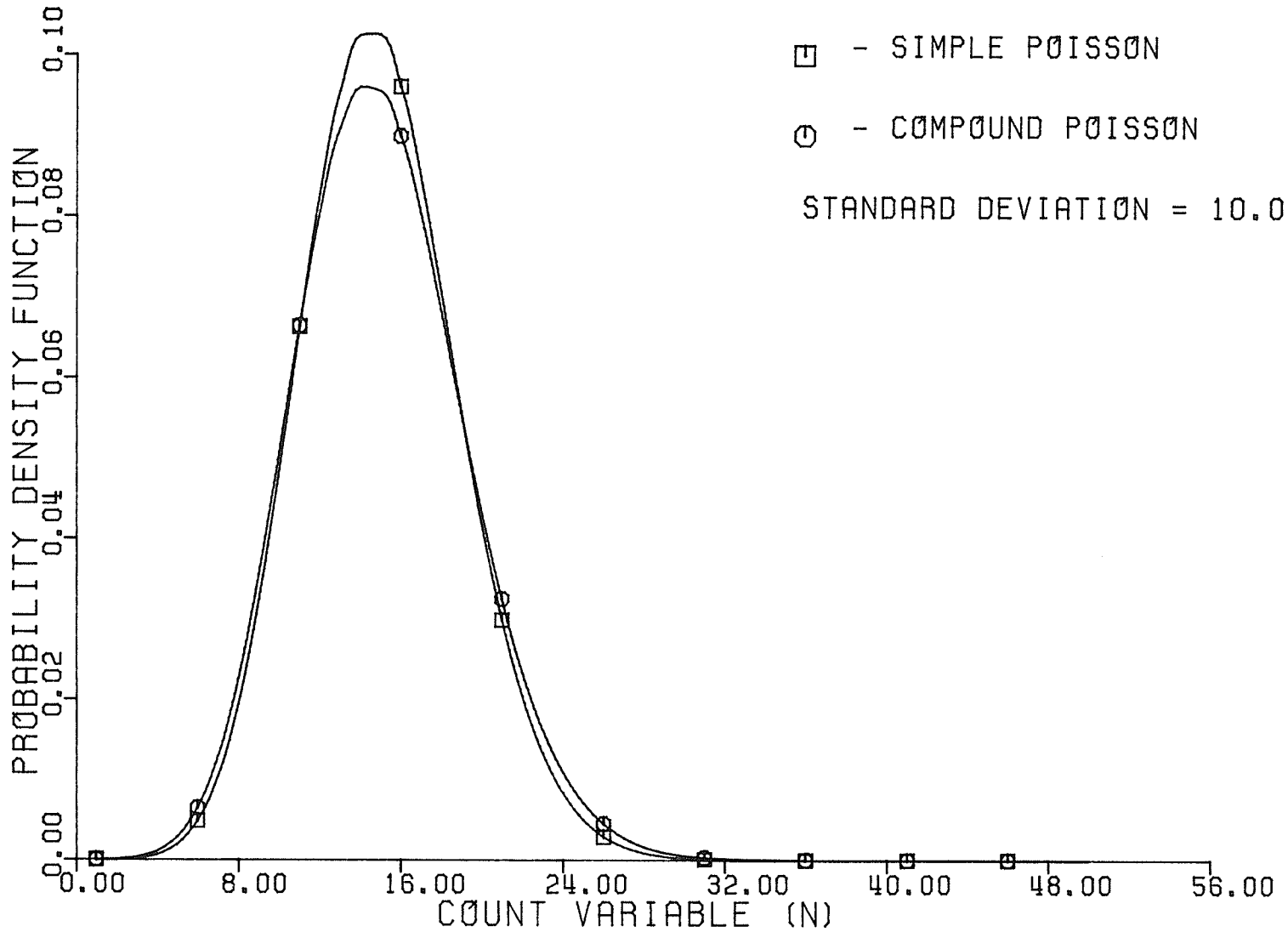

Figure 3.3: Photon probability density function, σ = 10.0 K

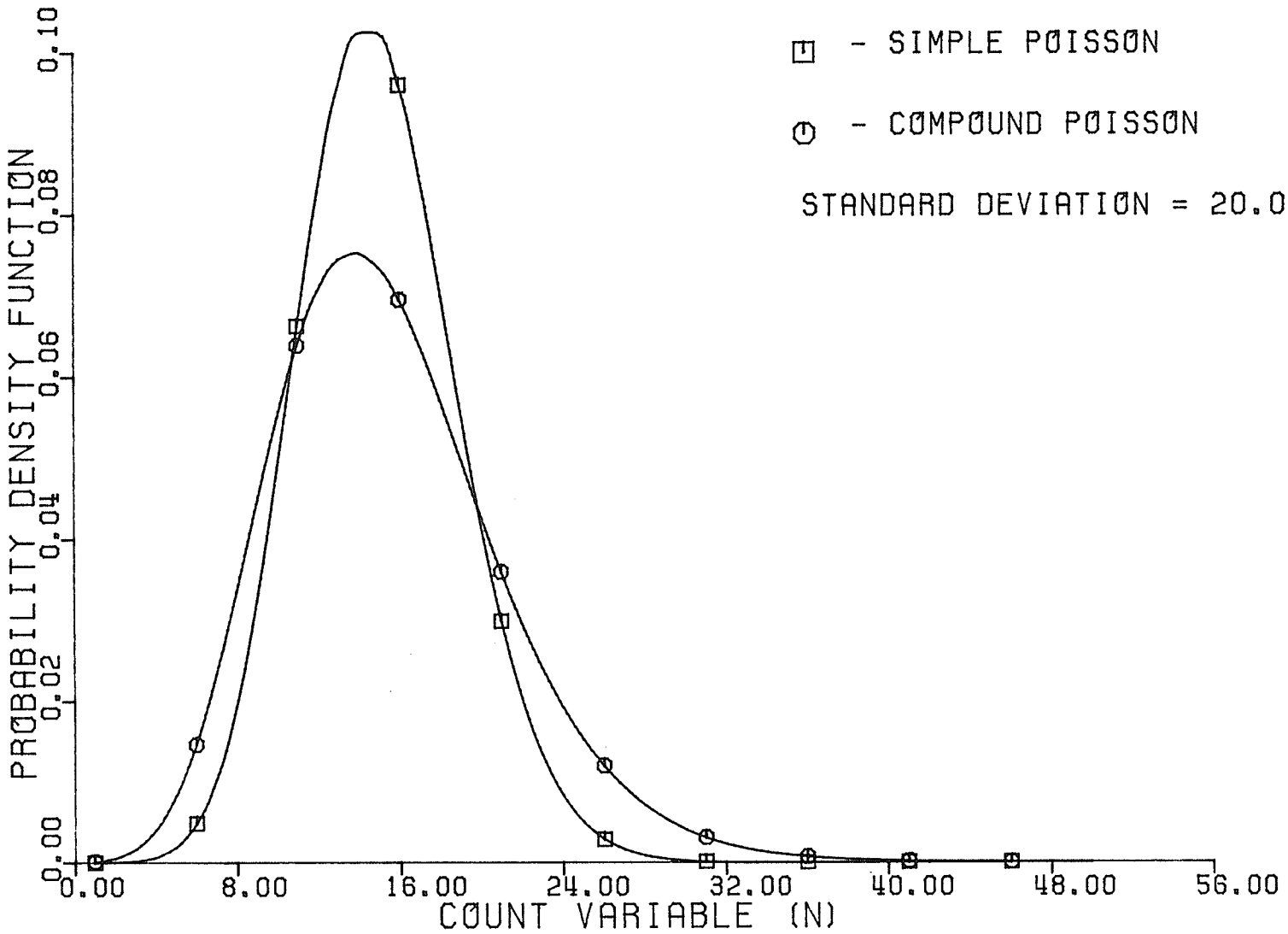

Figure 3.4: Photon probability density function, σ = 20.0 K

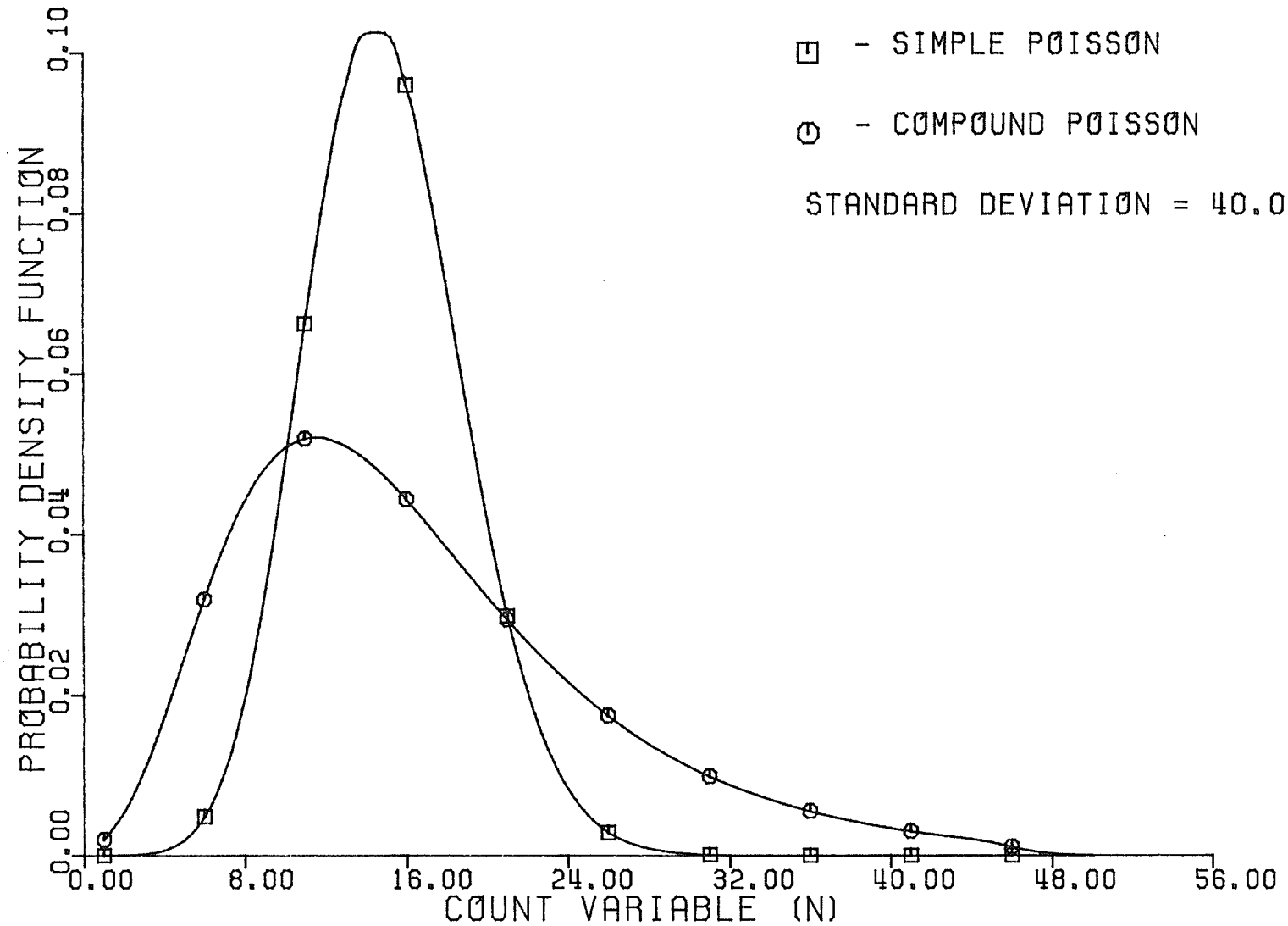

Figure 3.5: Photon probability density function, $\sigma = 40.0$ K

again the effect on the distribution will increase. The trend here shows that an increase in σ or a decrease in T_o (the latter of which is dependent upon the type of laser) will cause a downward shift in the mean and an overall asymmetric broadening of the probability density function.

At present there is no experimental data to support or refute this phenomenon. It seems however, that only for relatively large values of the standard deviation will this effect be seen. Under most circumstances the fluctuations in the temperature will be small, thus giving a relatively small standard deviation ($\sigma > 1.0$ K) for the fluctuations in the intensity. One might then assume that there will usually be other factors (i.e. reciever noise, amplifier noise, laser modal noise, etc.) involved in a system utilizing semiconductor lasers that will predominate over this small effect. In an unstable environment where large temperature fluctuations are possible the decreasing shift in the mean will most readily be observed.

It is important to recognize that photocounting statistics will only be employed for weak optical signals, so that count intervals will in many cases be over extended time periods. Even long term temperature fluctuations will therefore be important in the determination of the photocounting statistics.

Chapter IV

CONCLUSIONS

4.1 ON THE FRANZ-KELDYSH-PHOTOVOLTAIC OPTO-OPTIC MODULATOR

As was noted by Franz [2] and Keldysh [3], a increase in the electric field produces a dramatic increase in the absorption of optical radiation with photon energy in the neighbourhood of the energy gap (E_{gap}) of a semiconductor. By taking advantage of the photovoltaic effect in a semiconductor device such as a pn junction or a Schottky barrier a modification in the internal electric field can be produced by using an optical signal. By this principle the optical absorption of an optical signal in a semiconductor device can be modulated by using another optical signal. An optical signal with $\hbar\omega > E_{gap}$ is used for modulating the optical absorption of another signal $\hbar\omega < E_{gap}$.

The open-circuit voltage due to the photovoltaic effect of the control reduces the electric field decreasing the optical absorption coefficient within the space-charge region of the device, thereby enhancing the transmission of the signal with $\hbar\omega < E_{gap}$ through the space-charge region of the semiconductor.

For the appropriate choice of laser sources, and of the doping concentration of the modulator, a discrimination in

transmission ($T_{on} - T_{off}$) approaching unity is possible, for an integrated AlGaAs source/modulator system.

From the calculations presented in this thesis, we have shown the feasibility of a proposed 'opto-optic' modulator. Such a device is expected to have many interesting applications in digital or analog integrated optics.

4.2 ON THE TEMPERATURE DEPENDENCE OF SEMICONDUCTOR LASERS

For Gaussian temperature fluctuations the output intensity of a semiconductor laser will fluctuate. Usually these temperature fluctuations will be small and accordingly the standard deviation of the temperature distribution will be small. On the other hand, for sufficiently large temperature fluctuations (induced by unstable thermal environments or catrostrophic events) a substantial suppression of the mean count rate and a broadening of the photoelectron probability density function will be observed. For a nominal heat sink temperature of 350 K, a temperature fluctuation of approximately 10 K is sufficient to induce observable effects on the photocounting statistics.

REFERENCES

1) D.A. Buchanan and H.C. Card, 'Opto-Optic Modulation Based Upon a Photovoltaic Franz-Keldysh Effect in Semiconductors', IEEE J. Quant. Elect., submitted for publication

2) W. Franz, Z Naturforsch, 13, 484 (1958)

3) L.V. Keldysh, Soviet Physics - JETP 7, 788, (1958)

4) J. Calloway, "Optical Absorption in an Electric Field", Physical Review, 130, 548, (1963)

5) J. Calloway, "Optical Absorption in an Electric Field", Physical Review, 134, A998, (1964)

6) T.S. Moss, "Optical Absorption Edge in GaAs and its Dependence on Electric Field", J. Appl. Phys., 32, 2136, (1961)

7) L.M. Lambert, "Measurement of Optical Absorption in an Electric Field", Phys. Rev. B, 138, A1569, (1965)

8) E.G.S. Paige and H.D. Rees, "Absorption Edge of GaAs and Its Dependence on Electric Field", Phys. Rev. Lett., 16, 444, (1966)

9) J.I. Pankove, Optical Processes in Semiconductors , Dover Publications, New York, (1975), pp 47,303,313

10) S.M. Sze, Physics of Semiconductor Devices , Wiley Interscience, (1981), Ch.1,Part V

11) E.S. Yang, Fundementals of Semiconductor Devices , McGraw Hill, New York, (1978), pp 87-89

12) E.H. Rhoderick, Metal-Semiconductor Contacts , Oxford Science Publications, Clarendon Press, (1980), pp 94

13) M. Abromwitz and I.A. Segun, Handbook of Mathematical Functions , Dover Publications, New York, (1968), pp 446-449

14) M.A. Green, Solar Cells , Prentice Hall, pp.79 , 1982

15) W. van Roosbroeck and H.C. Casey Jr., "Transport in Relaxation Semiconductors", Phys. Rev. B, Vol.5, No.6, March 1972

15a) E.J. Johnson, J.kafalas, R.W. Davies and W.A. Dyes, "Deep Centre EL2 and Anti-Stokes Luminescence in Semi-Insulating GaAs", Appl. Phys. Lett., vol. 40, No. 11, pp.993, June 1982

16) H Kressel and J.K. Butler, Semiconductor Lasers and Heterojunction LED's , Academic Press, 1977, pp 360

17) H.C. Casey and M.B. Panish, Heterostructure Lasers : Part A - Fundamental Principles , Academic Press, 1978, pp 191-194

18) F.A. Jenkins and H.E. White, Fundamentals of Optics , McGraw Hill, 4th edition, (1976), pp 316-319

19) M.B. Panish, "Heterostructure Injection Lasers" , IEEE Proc., vol.64, No.10, October (1976)

20) D. Botez, "Contricted Double-Hetrostructure AlGaAs Diode Lasers : Structures and Electrooptical Characteristics", IEEE J. Quantum Electron., Vol QE-17, No.12, Dec 81

21) D.A. Buchanan and G. Gulak, 'Photon Counting Statistics Associated with Temperature Fluctuations in Semiconductor Lasers', J. Appl. Optics, submitted for publication

22) G.J. Troup, Photon Counting and Photon Statistics, Congress in Quantum Electronics, Pergamon Press, 1972

23) P. Daiment and M.C. Teich, 'Optical Detection of Laser or Scattered Radiation Transmitted Through the Turbulent Atmosphere', J. of Appl. Optics, vol. 10, pp. 1664, 1971

24) P. Daiment and M.C. Teich, 'Photoelectron-Counting Distributions for Irradiance-Modulated Radiation', J. Optical Soc. of America, Vol. 60, No. 5, 1970

25) P. R. Prucnal and M.C. Teich, 'Statistical Properties of Counting Distributions for Intensity Modulated Sources', J. Optical Soc. of America, vol. 69, No. 4, 1979

26) T.L. Paoli, 'Noise Characteristics of Stripe-Geometry Double-Heterostructure Junction Lasers Operating Continuously -1. Intensity Noise at Room Temperature', IEEE J. of Quantum Electron., vol. QE-11, No. 6, 1975

27) T.L. Paoli, 'Intrinsic Fluctuations in the Output Intensity of Double-Heterostructure Junction Lasers Operating Continuously at 300 K', Appl. Phys. Lett., vol. 24, No. 4, 1974

28) H.C. Casey Jr. and M.B. Panish, Heterostructure Lasers, Part A Fundamantal Principles, Academic Press, pp. 46-47, 1978

29) S.M. Sze, Physics of Semiconductor Devices - 2nd Edition, Wiley-Interscience, New York, pp.731, 1981

30) W.T. Tsang,,R.A. Logan and J.P. Van der Ziel, 'Low Current Threshold Stripe-Buried-Heterostructure Lasers with Self-Aligned Current Injection Stripes', Appl. Phys. Lett., vol 34, pp. 644, 1979

31) N.K. Dutta and R.J. Nelson, 'Temperature Dependence of the Lasing Characteristics of 1.3 μm InGaAsP - In and GaAs - $Al_x Ga_{1-x}$ As DH Lasers', IEEE J. of Qunatum Electron., vol QE-18, pp. 871 May, 1982

32) Y. Horikoshi and Y. Furukawa, 'Temperature Sensitive Threshold Current of InGaAsP - InP Double Heterostructure Lasers', Japan J. Appl. Phys., vol. 18, pp. 809, Apr. 1979,

33) G.H.B. Thompson and G.D. Henshall, 'Nonradiative Carrier Loss and Temperature Sensitivity of 1.27 μm InGaAsP - InP DH Lasers', Electron. Lett., vol. 16, pp. 42, 1980

34) N.K. Dutta and R.J.Nelson, 'Temperature Dependence of the Threshold of InGaAsP DH Lasers and Auger Recombination', Proc. Int. Symp. GaAs. and Related Compounds, Vienna, Austria, Sept. 22-24, 1980, Inst. of Phys., Conf. Series No. 56, pp.193

35) _____, 'Temperature Dependence of Threshold of InGaAsP-InP Double Heterostructure Lasers and Auger Recombination', Appl. Phys. Lett., vol. 38, pp. 407, Mar., 1981

36) A. Sugimura, 'Band to Band Auger Recombination Effect on InGaAsP Laser Thershold', IEEE J. Quantum Electron.. vol. QE-17, pp. 627, May, 1981

37) T.U.K. Iwamoto and R.Lang, 'Nonradiative Recombination in InGaAsP - InP Light Sources Causing Light Emitting Diode Output Satureation and Strong Laser-Threshold-Current Temperature Sensitivity', Appl. Phys. Lett., vol. 38, pp. 193, Feb., 1981

38) N.K. Dutta, 'Temperature Dependence of Threshold Current of GaAs-$Al_x Ga_{1-x}$ As Double Heterostructure Lasers', J. Appl. Phys., vol. 52, pp. 70, 1981

39) A. Papoulis, Probability, Random Variables and Stochastic Processes McGraw-Hill, pp. 65,98-111, 1965

40) M.H. Lean, 'Electromagnetic Field Solution with the Boundary Element Method', PhD Disertation, Dept. of Elect. Engineering, University of Manitoba, pp 22-27, 1981

Appendix A

SPECTRAL RESPONSE OF A SHORT RANGE FIBREOPTIC DATA LINK

A.1 INTRODUCTION

During the past few years, the development in fibre optic technology has been extensive. Today optical fibres represent a high-speed, low noise and cost effective solution to the data communication problem. When compared with the conventional, paired communication channel (i.e. telephone lines), the advantages of the fibre-optic link become apparent. Fibres are much less suseptible to electromagnetic or radio-frequency interference, and can isolate a system against high voltages. Also due to the physical nature of the transmission medium, the fibre-optic system can provide secure data communications. As to the data rates of currently available systems, the restrictions are often in the transmitters and/or the receivers and not in the fibre medium itself. Fibre communication also represents a system with almost unlimited bandwidth. Frequency multiplexing can provide fairly large use of this bandwidth; however, the availabilty of optical sources and arrays of sources is limited.

There are many different types of fibreoptic systems that can be used for applications that are currently of interest.

Probably the two most universal applications are 1) high speed data communication (i.e. a telephone network or long range computer network) and 2) short range computer communications.

This appendix reports the results of an experimental investigation of the optical characteristics of one specific short range fibre system. This study was conducted on the Hewlett-Packard HFBR-0500 system. This system includes an LED transmitter, an integrated photodetector-amplifier receiver and a 5m length of plastic fibre. The experiments were conducted to identify the spectral characteristics of the operational system and to determine the efficiency of the design. While this study was not intended as research, it was decided to include it in the thesis as an accessible data base for a graduate laboratory experiment, and as such a contribution to the study of optoelectronic systems.

A.2 MEASUREMENTS AND RESULTS

In determination of the optical characteristics of this system the power density spectrum of the fibre and the LED source were obtained. Unfortunately due to the integrated nature of the receiver, its operating characteristics could not be directly measured. The photodetector in isolation was not accessible. Only the output of the preamplifier, integrated on the same chip as the detector, was measurable. The circuit also incorporated a level detector so its output

was either a high or low state, and therefore no specific operating characteristics of the photodetector itself could be obtained.

The system that was used to perform these experiments is shown in figure A.1 . A Xenon light source (Photochemical Research 303X) was used and the power density was measured as a function of wavelength using a monochromator (American ISA Inc. H10-V16) and a photometer (Optikon model 550-1). A normalizing filter was also used to compensate the variation in sensitivity of the photometer over the interval of wavelengths.

The measuring system (Fig. A.1 (a)) was first calibrated as a function of wavelength. Figure A.2 shows the results of these measurements.

The fibre was then placed between the Xenon source and the monochromator. The same procedure was repeated. The raw data of the measurement (not taking into account the calibration) is shown in Fig. A.3 .

All of the measurements that were taken on this system were measured in units of watts/cm . The diagrams that were constructed from the measured data are normalized with respect to the maximum value.

If we call the response of the measurement system X(f) and the raw response tf the fibre and the measurement system Y(f) and the transfer function (or the actual fibre characteristic) H(f), then the fibre characteristic H(f) can be given by

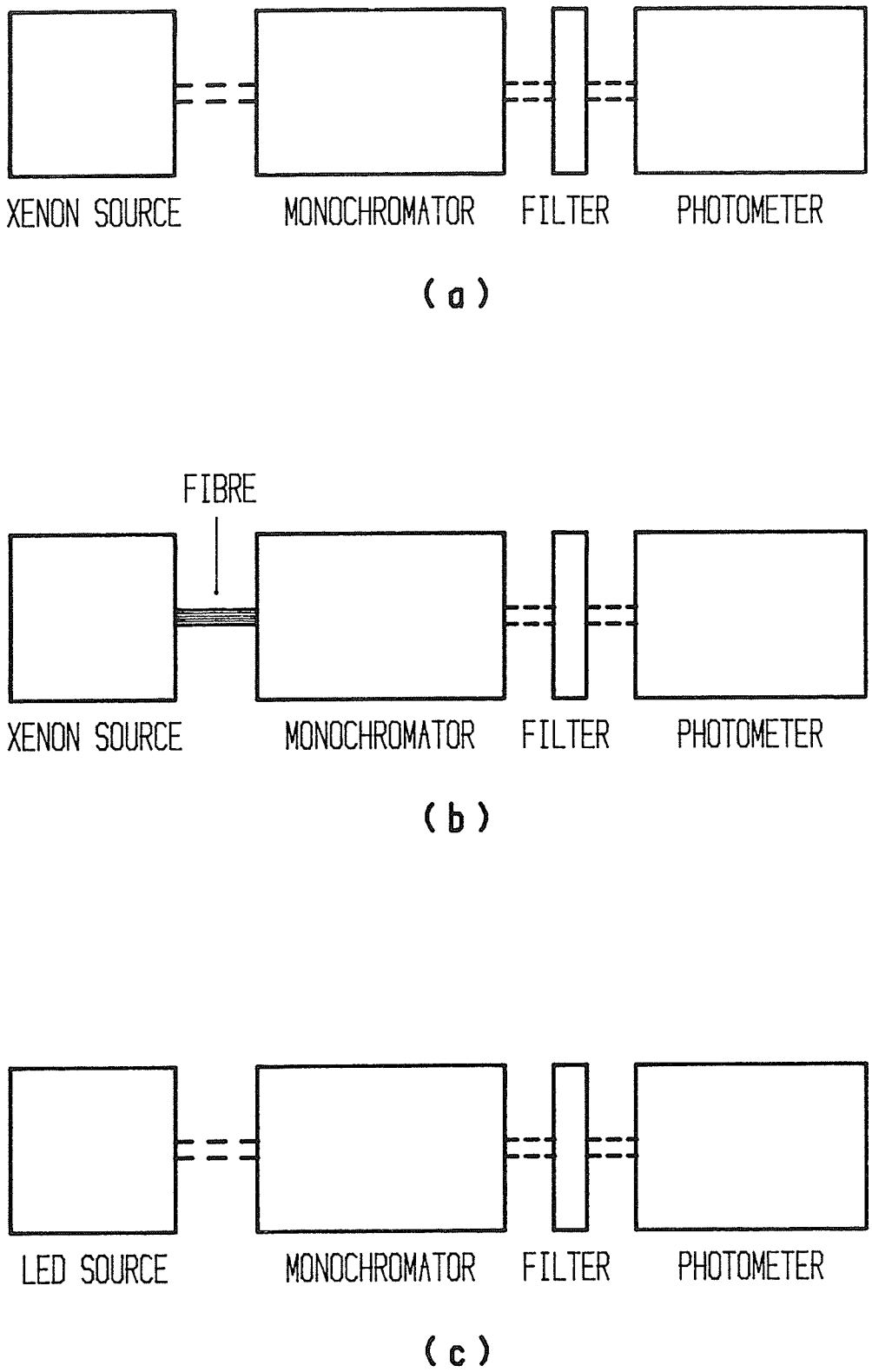

Figure A.1: Measurement system for determination of the optical characteristics of the HP data link.

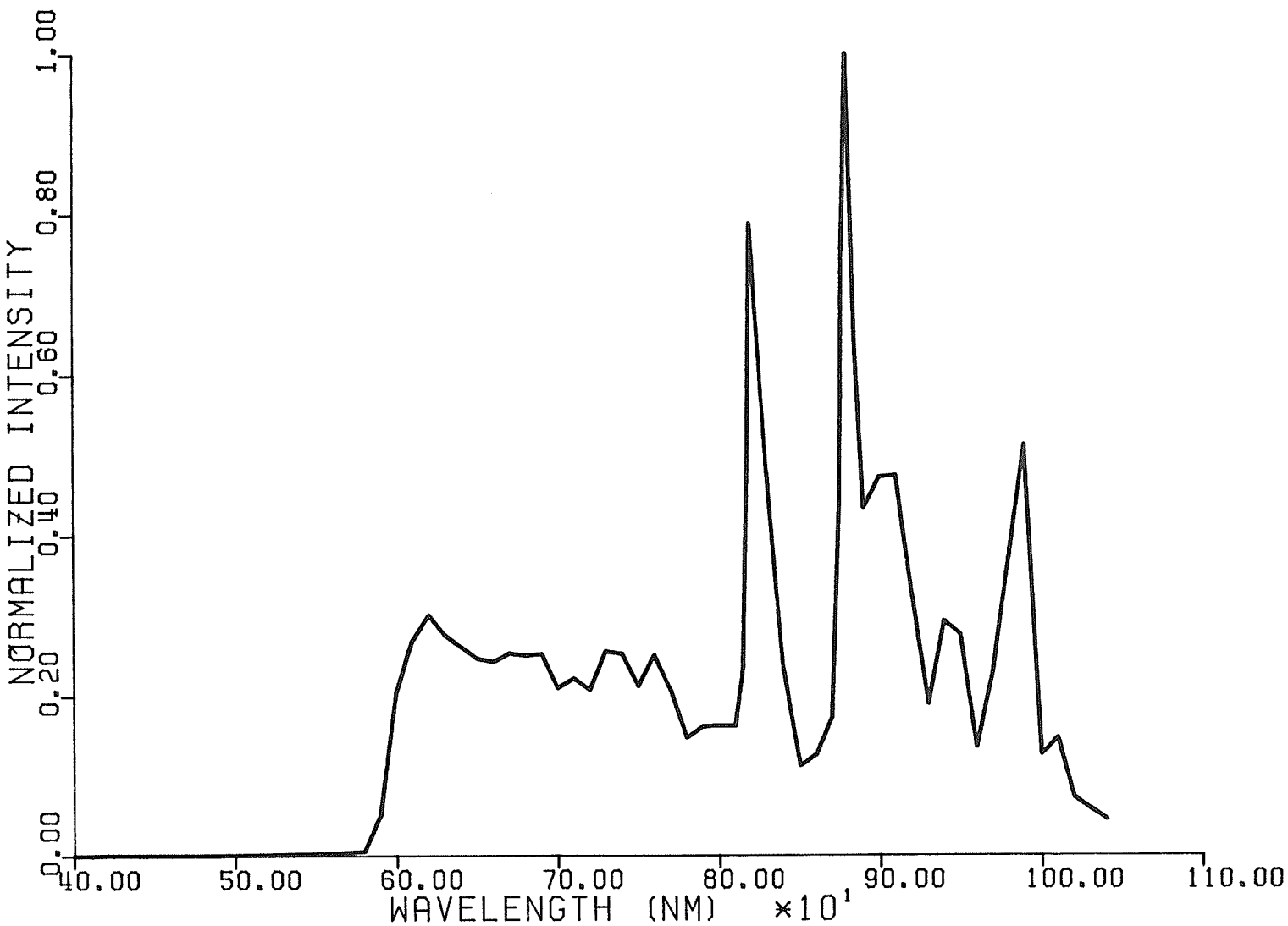

Figure A.2: Calibration spectral density of the measurement system.

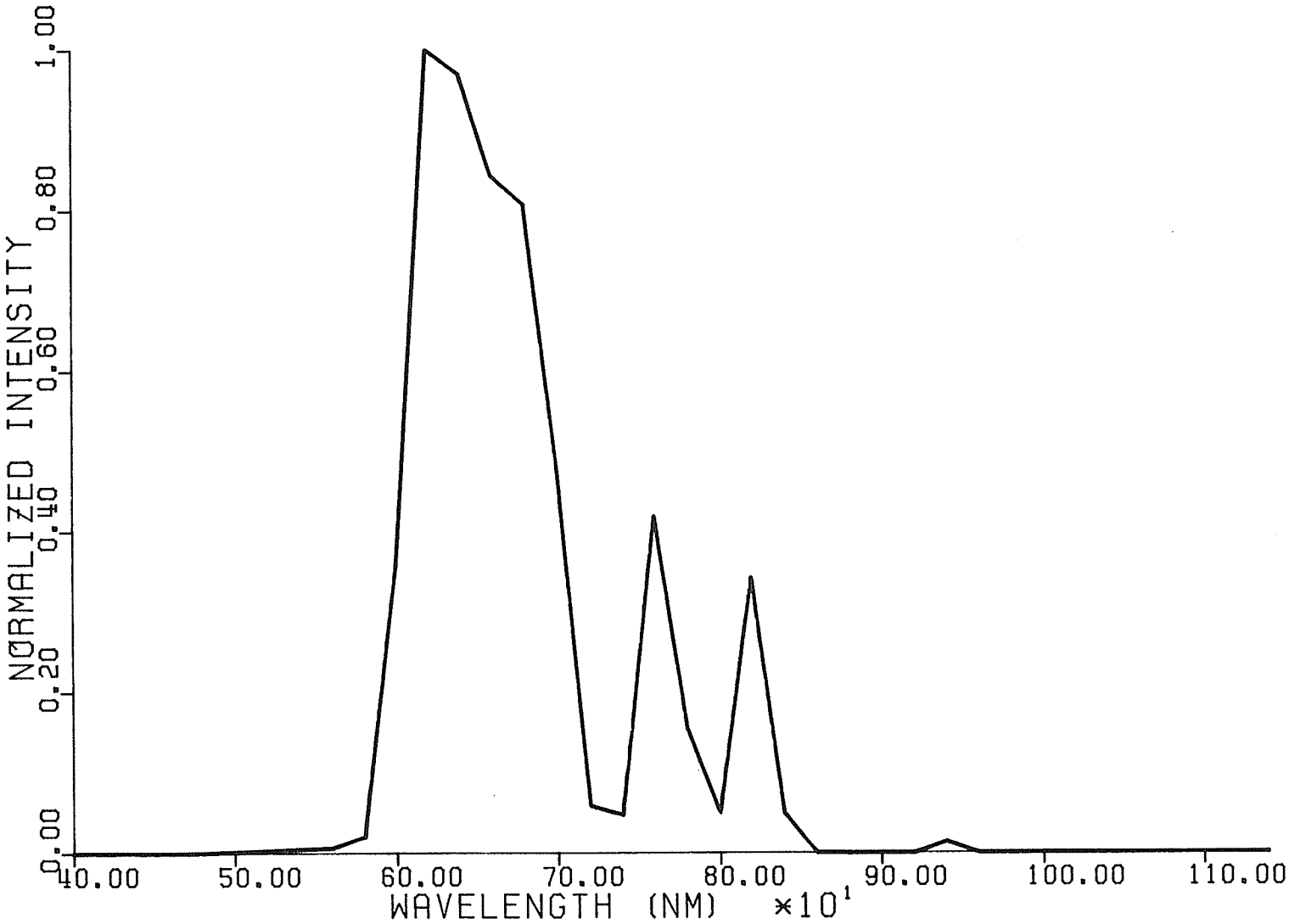

Figure A.3: Measured spectral density of system and fibre combined.

$$H(f) = \frac{Y(f)}{X(f)} \qquad (A.1)$$

Figure A.4 shows the actual spectral response of the fibre as given by Eqn. 4.1.

The measurement of the LED transmitter characteristic was done in a similar way as that of the fibre measurement. The LED in this case was placed at the input side of the monchromator and the Optikon detector was placed at the output. Measurements were then taken of the power density of the LED output as a function of wavelength. This is shown in Fig. A.5

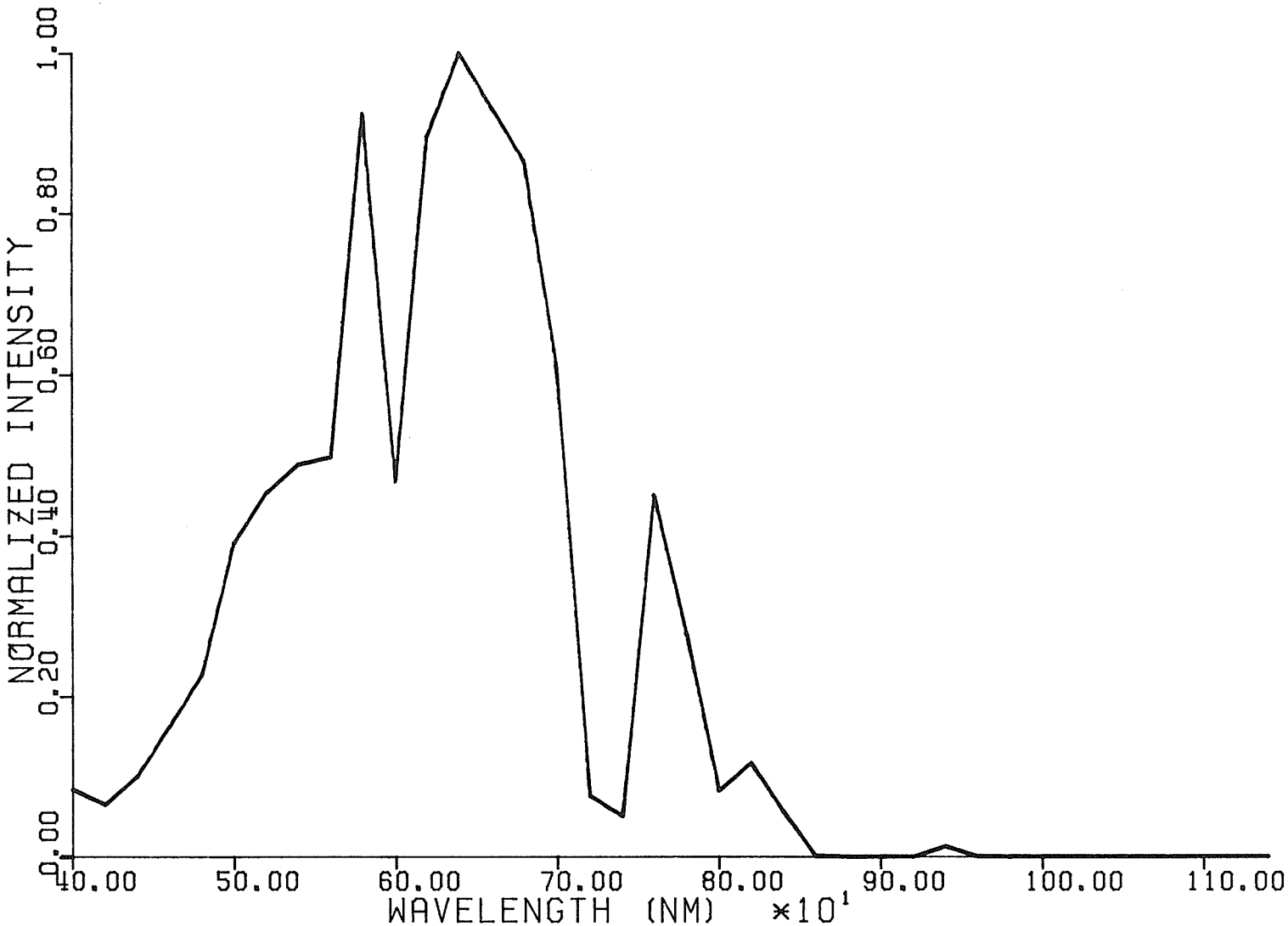

Figure A.4: Spectral response of the HP plastic fibre.

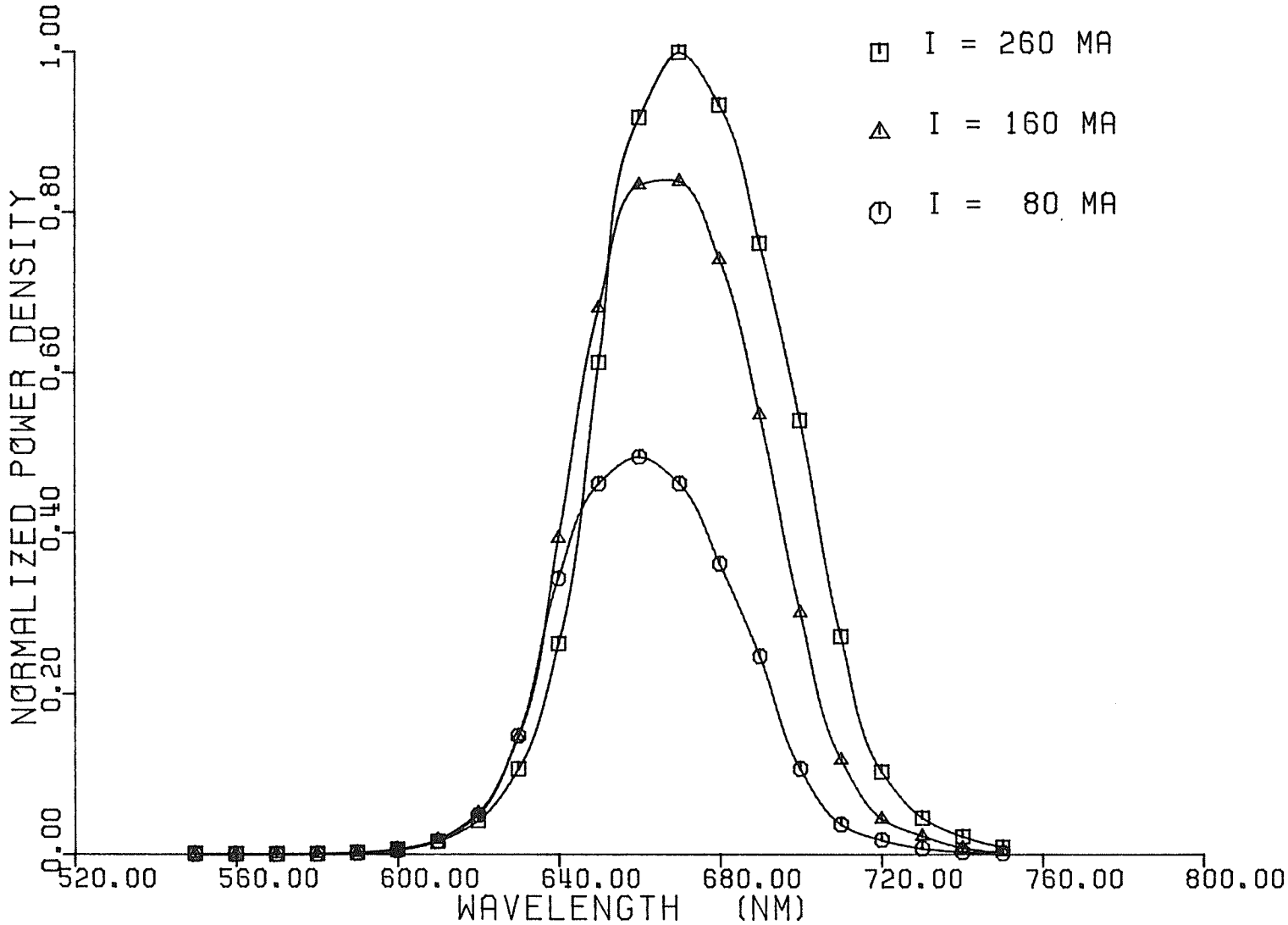

Figure A.5: Power density spectrum of the LED source for three different drive currents, 80 mA, 160 mA and 260 mA.

A.3 RESULTS AND DISCUSSION

In a fibre optic system, as in any communication system, the matching of the component characteristics will be important to the overall performance. In this experimental study we were interested solely in the optical characteristics, specifically the spectral response of each of the components. Ideally all of the parts would have been tested but due to the integrated nature of the receiver, this was not possible.

Figure A.5 shows the power density spectrum of the output of the LED source for three different drive currents. The peak recomended drive current is 60 mA. We found that at considerably larger currents no substantial degradation was noticed. However, long term degradation was not one of the objectives of this investigation.

The main purpose in driving the source at different levels was to determine any shifts in the peak wavelength. For low drive levels, the peak was found at 660 nm, close to that stated in the data sheets (665 nm). There was however a noticable shift in the peak at larger drive currents. At 200 mA the peak was at 672 nm. This shift is probably due to the increase in device temperature with increased drive current. A shift in the energy gap of the LED material is probably responsible. In the neighborhood 300 K, the temperature coefficient of the energy gap of GaAsP is approximately -0.0005 eV/K. For a shift of 12 nm in peak wavel-

ength, the temperature increase is approximately 20 K, a reasonable value to expect under the increased drive current.

For the best system efficiency, one would expect the spectral response of the fibre to peak at approximately the same wavelength as the source. A comparison of Figs. A.4 and A.5 shows this to be the case. The response of the fibre was found to peak at about 620 nm. At 665 nm the normalized intensity was 0.92, very close to the maximum (1.0). It seems that the system is matched well optically.

A.4 CONCLUSIONS

For this kind of a communication system to work at peak efficiency, the spectral response of the fibre should be spectrally matched to the LED source. The HBFR-0500 system accomplishes this match relatively well. The response of the fibre was found to peak at 620 nm, and at the peak of the output of the source (660 nm) the normalized intensity of the fibre was 0.92. The silicon photodetector also exhibits close to maximum sensitivity in this range of wavelengths.

Appendix B

PROGRAM LISTING FOR OPTO-OPTIC MODULATOR

```
//OPTOMOD  JOB ',,,T=9',BUCHANAN
// EXEC WATFIV
//GO.SYSIN DD *
CJOB WATFIV BUCHANAN,NOEXT
C
C     ******************************************************
C
C     DECLARATION OF VARIABLES ( 1ST SECTION )
C
C    ********************************************************
C
C     FPH = INTENSITY (OF BEAM 1) IN PHOTONS/CM**2/S
C
C     EPH = PHOTON ENERGY (OF BEAM 2) IN ELECTRON VOLTS
C           (EPH1 IS JUST A HOLDING VALUE OF EPH)
C
C      VOC = OPEN CIRCUIT VOLTAGE
C
C      VT  = THERMAL VOLTAGE ( 0.026 V )
C
C      VN  = BUILT IN POTENTIAL
C
C      VDMAX,VDMIN = MAXIMUM AND MINIMUM DIFFUSION POTENTIAL
C
C      Q   = ELECTRONIC CHARGE
C
C      ER  = RELATIVE PERMITTIVITY OF GaAs
C
C      EO  = PERMIATIVITY OF FREE SPACE
C
C      PHIB = SCHOTTKY BARRIER HEIGHT
C
C      DOPE,DOPING = DOPING CONCENTRATION PER CM**2 AND
C                    PER M**2 RESPECTIVLY
C
C      EMAX,EMIN = MAXIMUM AND MINIMUM ELECTRIC FIELD
C
C      W  = DIFFUSION WIDTH
C
C      W0 = APERTURE OF SAMPLE TO BEAM 2
C
C      ALL OTHER VARIABLES IN THE FIRST SECTION ARE
C      STORAGE VALUES IN INTERMEDIATE STEPS OR FOR
C      PRINT OUT.
```

```
C
C
C     ******************************************************
C
      REAL*8 FPH,CNOT,EPH2,VOC,VT,PHIB,VN,Q,CPH,ER,E0,
     &DOPING,EMAX,W,W0,PER,FPH0,FPH2,DE,SUM,AVE,EMIN,AREA,
     &DOPE,FPH2MN,FPH2MX,HDPER,PERH,PERL,DPER,HEPH1,HDOPE,
     &E1,E2,A1,A2,VDMAX,VDMIN
C
C     ******************************************************
C
C      YO = VARIABLE FOR AIRY INTEGRAL
C
C      C1,C2 = AIRY INTEGRAL CONSTANTS
C
C      FACTF,FACTG = FACTORIAL CALCULATIONS
C
C      RSTMAS = REST MASS OF AN ELECTRON
C
C      EFIELD = ELECTRIC FIELD
C
C      EGAP = ENERGY GAP OF GaAs (1.43 eV)
C
C      ALMBDA = WAVELENGTH OF BEAM 2
C
C      ALPHA = ABSORPTION COEFFICIENT
C
C      H = PLANCK CONSTANT
C
C      ALL OTHER VARIABLES IN THIS SECTION ARE CONSTANTS
C      OR REPRESENT INTERMEDIATE STEPS
C
C     ******************************************************
C
      REAL*8 YO,C1,C2,AIZ,FZ,GZ,DFZ,DGZ,FCOUNT,GCOUNT,
     &ZF,ZG,FACTF,FACTG,DAIZ2,PI,RSTMAS,EFIELD,U,BETA,CYO,
     &HPLNKS,EGAP,EPH1,ALMBDA,ALPHA,AK,MNU,H
C
C     ******************************************************
C
C     INITIALIZATION OF CONSTANTS
C
      EPH2=2.0
      FPH0=1.0D2
      FPH2MX=1.2D1
      FPH2MN=-1.0
      PHIB=0.95
      VT=0.026
      CNOT=5.36D-9
      Q=1.602D-19
      ER=10.9
      E0=8.854D-12
      DENC=4.17D17*(1.0D8)
      HDPER=0.0
```

```
      VDMAX=0.70D0
      VDMIN=0.20D0
C
C
C
      DOPE=1.0D13
      WHILE (DOPE.LE.1.0D17) DO
      PRINT 050
      EPH1=.140D1
      WHILE (EPH1.LE..145D1) DO
C
      DOPING=DOPE*(1.0D6)
C
C
      NCT=1
      VD=VDMAX
      WHILE (NCT.LE.2) DO
C
C      CALCULATION OF MAXIMUM ELECTRIC FIELD AND DIFFUSION
C      WIDTH
C
C
C
         W0=(2*E0*ER/Q/DOPING*(VD))
         W=DSQRT(W0)
         EMAX=Q*DOPING*W/ER/E0
C
C
C     CALCULATION OF INTEGRATION OF TOTAL ABSORPTION OF THE
C     ENTIRE SAMPLE
C
C
         EMIN=EMAX/10
         N=10
C
C     ************************************************************
C
         DE=(EMAX-EMIN)/N
         EFIELD=EMIN
         FPH=FPH0
C
C
  10     H=(EMAX-EMIN)/N
         SUM=.0D0
         EFIELD=EMIN+H
         DO 4 I=2,N
         IF(MOD(I,2))2,2,3
  2      SUM=SUM+4.0*(ALPHA(EFIELD,EPH1))
         GO TO 4
  3      SUM=SUM+2.0*(ALPHA(EFIELD,EPH1))
  4      EFIELD=EFIELD+H
         AREA=H/3.0*(ALPHA(EMAX,EPH1)+SUM
     &  +ALPHA(EMIN,EPH1))
         AREA=AREA*W/EMAX
```

```
C
C       CALCULATION OF OUTPUT VALUES FOR STORAGE FROM THE
C       VALUE OF THE INTEGRATION
C
          IF(DABS(AREA).GT.160.0) THEN DO
             FPH=.0D0
          ELSE DO
             FPH=FPH0*(DEXP(-AREA))
          END IF
          PER=(FPH/FPH0)*100.0
          IF(NCT.EQ.1) THEN DO
             PERH=PER
             E1=EMAX
             A1=AREA
          ELSE DO
             PERL=PER
             E2=EMAX
             A2=AREA
          END IF
C
          VD=VDMIN
          NCT=NCT+1
          PRINT 075
       END WHILE
       DPER=(PERH-PERL)
       EPH11=EPH1
       IF (DPER.GT.HDPER) THEN DO
          HDPER=DPER
          HEPH1=EPH1
          HDOPE=DOPE
       END IF
       PRINT 100,PERH,E1,A1,PERL,E2,A2,EPH1,DOPE
       PRINT 075
       DPERR=DPER
       PERHH=PERH
       PERLL=PERL
       EPH1=EPH1+0.01
       END WHILE
       DOPE=DOPE*1.0D1
       END WHILE
C
  050 FORMAT('1')
  075 FORMAT('0')
  100 FORMAT('0',D14.6,D14.6,D14.6,D14.6,D14.6,D14.6,D14.6,D14.6)
  200 FORMAT('1',D18.8,D18.8,D18.8)
C
       STOP
       END
C
C
C
C      ************************************************************
C
C       FUNCTION ROUTINE TO CALCULATE THE ABSORPTION COEFFICIENT
```

```
C       FOR THE INTEGRATION AT ANY POINT IN THE SAMPLE
C
C      ************************************************************
C
C
      FUNCTION ALPHA(EFIELD,EPH1)
C
      REAL*8 YO,C1,C2,AIZ,FZ,GZ,DFZ,DGZ,FCOUNT,GCOUNT,
     &ZF,ZG,FACTF,FACTG,DAIZ2,PI,RSTMAS,EFIELD,U,BETA,CYO,
     &HPLNKS,EGAP,EPH1,ALMBDA,ALPHA,AK,MNU,EMIN,EMAX,FPH
C
      PI=ARCOS(0.0)*2.0
      RSTMAS=9.1D-31
      HPLNKS=6.626D-34/(2*PI)
      EGAP=1.43
      AK=4.10D20
C
      ALMBDA=1.24/EPH1
      MNU=3.0D8/ALMBDA
C
      U=0.068*0.56/(0.068+0.56)*RSTMAS
      BETA=2*U*EFIELD*1.602D-19/HPLNKS**2
C
      CYO=2*U/(HPLNKS**2)/(BETA**(0.66666667))
C
C
      YO=CYO*(EGAP-EPH1)*1.602E-19
      IF(DABS(YO).LE.5.0D-3)YO=.0D0
C
C
      C1=0.355028053887817
      C2=0.258819403792807
C
      GZ=YO*C2
      FZ=C1
C
      ZF=1.0
      ZG=1.0
C
      DFZ=0.0
      DGZ=C2
      DAIZ2=DFZ-DGZ
C
      AIZ=FZ-GZ
      K=1
C
      WHILE (K.LE.5) DO
         FCOUNT=3*K-2
         GCOUNT=3*K-1
C
         ZF=ZF*FCOUNT
         ZG=ZG*GCOUNT
C
         NEXPF=3*K
```

```
          NEXPG=(3*K)+1
C
          NDEXPF=NEXPF-1
          NDEXPG=NEXPG-1
C
          N=1
          FACTF=1.0
          WHILE (N.LE.NEXPF) DO
             FACTF=FACTF*N
             N=N+1
          END WHILE
C
          N=1
          FACTG=1.0
          WHILE (N.LE.NEXPG) DO
             FACTG=FACTG*N
             N=N+1
          END WHILE
C
          FZ=C1*((ZF/FACTF)*(YO**NEXPF))
          GZ=C2*((ZG/FACTG)*(YO**NEXPG))
C
          AIZ=AIZ+(FZ-GZ)
C
          DFZ=C1*((ZF*3*K)/FACTF)*(YO**NDEXPF)
          DGZ=C2*((ZG*(3*K+1))/FACTG)*(YO**NDEXPG)
          DAIZ2=DAIZ2+(DFZ-DGZ)
C
C
          K=K+1
       END WHILE
C
       IF(YO.GT.10.)AIZ=0.
       IF(YO.GT.10.)DAIZ2=0.
       DAIZ2=DAIZ2**2
       ALPHA=AK*(BETA**(0.3333333))*MNU*U*(DAIZ2-YO*AIZ**2)
       PRINT 300,YO,AIZ,DAIZ2,ALPHA,EFIELD
C
C      ***********************************************************
C
  300  FORMAT(' ',D18.8,D18.8,D18.8,D18.8,D18.8)
C
       RETURN
       END
CNTRY
//FT11F001 DD DSN=dataset name,DISP=SHR
//FT12F001 DD DSN=dataset name,DISP=SHR
//FT13F001 DD DSN=dataset name,DISP=SHR
```

Appendix C

PROGRAM LISTING FOR PHOTON STATISTICS CALCULATION

```
//CPSN   JOB ',,,T=20',BUCHANAN
// EXEC WATFIV
//GO.SYSIN DD *
CJOB WATFIV BUCHANAN,NOEXT
C
C     ***********************************************************
C     *                                                         *
C     *      THIS PROGRAM IS USED FOR THE CALCULATION OF        *
C     *      OF COMPLEX POISSON STATISTICS AS RELATED TO        *
C     *      TO THE TEMPERATURE FLUCTUATIONS IN                 *
C     *      SEMICONDUCTOR LASERS                               *
C     *                                                         *
C     ***********************************************************
C     *                                                         *
C     *      THIS PROGRAM USES A FUNCTION TO MODULATE           *
C     *      THE AVERAGE VALUE OF THE SIMPLE POISSON            *
C     *      STATISTICS. THIS FUNCTION CAN TAKE ANY             *
C     *      FORM. IN THIS CASE HOWEVER THE MODULATION IS       *
C     *      STOCHASTIC.                                        *
C     *                                                         *
C     ***********************************************************
C     ***********************************************************
C     *                                                         *
C     *       DEFINITION OF VARIABLES                           *
C     *                                                         *
C     *   XMIN -- THE LOWER LIMIT OF THE INTEGRATION OF THE     *
C     *           PRODUCT OF THE STOCHIASTIC MODULATION OF      *
C     *           THE AVERAGE OR MEAN LASER INTENSITY AND       *
C     *           THE SIMPLE POISSON DENSITY FUNCTION FOR       *
C     *           A GIVEN MEAN VALUE.                           *
C     *   NOTE : |XMIN-XNOT|`13   OR EXPONENT UNDER FLOW        *
C     *                                                         *
C     *   XMAX -- AS ABOVE EXCEPT THAT THIS IS THE UPPER        *
C     *           LIMIT OF THE INTEGRATION.                     *
C     *                                                         *
C     *   N ----- THE NUMBER OF INTEGRATION AREAS OVER THE      *
C     *           RANGE FROM XMIN TO XMAX.                      *
C     *                                                         *
C     *   H ----- THE INTEGRATION STEP SIZE                     *
C     *                                                         *
C     *   X ----- THE VARIABLE OF INTEGRATION                   *
C     *                                                         *
C     *   SUM --- PARTIAL SUM OF THE TOTAL AREA OF              *
C     *           INTEGRATION                                   *
```

```
C     *   SUM --- PARTIAL SUM OF THE TOTAL AREA OF                *
C     *           INTEGRATION                                     *
C     *                                                           *
C     *   AREA -- THE TOTAL AREA OF INTEGRATION                   *
C     *                                                           *
C     *   MSAVE - THE RANDOM POISSON COUNTING VARIABLE            *
C     *                                                           *
C     *   MSMAX - THE MAXIMUM VALUE FOR THE POISSON RANDOM        *
C     *           VARIABLE SO AS TO BE WRITTEN INTO THE           *
C     *           DATASET FOR PLOTTING.                           *
C     *                                                           *
C     *                                                           *
C     *    ----------------------------------------------         *
C     *                                                           *
C     *    DUMMYF(X,MSAVE,NSIGMA) IS THE STOCHASTIC               *
C     *    MODULATION FUNCTION.                                   *
C     *                                                           *
C     *    THE FOLLOWING ARE VARIABLES APPLYING TO THIS           *
C     *    FUNCTION.                                              *
C     *                                                           *
C     *    XNOT --- THE AVERAGE OR MEAN VALUE OF THE ORIGINAL     *
C     *             POISSON DISTRIBUTION                          *
C     *                                                           *
C     *************************************************************
C
C
      XMIN=1.E-5
      XMAX=50.
      N=300
      MSMAX=45
      NONE=1
C
C     ------------------------------------------------------------
C
      WRITE(11,*)MSMAX
      WRITE(11,*)NONE,NONE
      Y=15
      MSAVE=1
      WHILE (MSAVE.LE.MSMAX) DO
         POIS=Y**MSAVE*EXP(-Y)
         M=1
         FACTM=1
         WHILE(M.LE.MSAVE) DO
            FACTM=FACTM*M
            M=M+1
         END WHILE
         POIS=POIS/FACTM
         WRITE(11,*)MSAVE,POIS
         MSAVE=MSAVE+1
      END WHILE
C
      MSAVE=1
      WHILE (MSAVE.LE.MSMAX) DO
C
```

```
C     ------------------------------------------------------------
C
C     THE FOLLOWING ROUTINE PERFORMS THE INTEGRATION OF THE
C     PRODUCT OF THE MODULATION FUNCTION AND THE POISSON
C     FUNCTION OVER THE RANGE XMIN TO XMAX.
C
C     ------------------------------------------------------------
C
  10  H=(XMAX-XMIN)/N
      SUM=0.
      X=XMIN+H
      DO 4 I=2,N
      IF(MOD(I,2))2,2,3
  2   SUM=SUM+4.*(DUMMYF(X,MSAVE))
      GO TO 4
  3   SUM=SUM+2.*(DUMMYF(X,MSAVE))
  4   X=X+H
      AREA=H/3.*(DUMMYF(XMIN,MSAVE)+SUM
     &+DUMMYF(XMAX,MSAVE))
      WRITE(11,*)MSAVE,AREA
      MSAVE=MSAVE+1
      END WHILE
  50  CONTINUE
      STOP
      END
C
C     ------------------------------------------------------------
C
C        THE FOLLOWING BLOCK DESCRIBES ALL VARIABLES AND
C        CONSTANTS NEEDED FOR THE CALCULATION OF THE MODULATION
C        FUNCTION
C
C     ------------------------------------------------------------
C
      FUNCTION DUMMYF(X,MSAVE)
      PI=ARCOS(0.)*2.
      XNOT=15.
      SIGMA1=.66666667
      TONE=60.
      SIGMA=SIGMA1*TONE
      A=1/(X*SQRT(2.*PI)*SIGMA1)
      M=1
      FACTN=1
      WHILE (M.LE.MSAVE) DO
         FACTN=FACTN*M
         M=M+1
      END WHILE
C
C
      ARG=-(ALOG(X/XNOT))**2/(2*SIGMA1**2)
      IF (ABS(ARG).GT.172) THEN DO
         B=1.E-78
         B1=ALOG10(B)
      ELSE DO
```

```
         B=A*(EXP(ARG))
         B1=ALOG10(B)
      END IF
      ANUM=MSAVE*ALOG10(X)
      IF(ANUM.LT.0..AND.ANUM.LT.-78) THEN DO
         C=1.E-78
      ELSE DO
         IF ((MSAVE*ALOG10(X)).GT.75) THEN DO
            C=1.E75
         ELSE DO
            C=X**MSAVE
         END IF
      END IF
      IF (X.GT.172) THEN DO
         D=1.E-78
      ELSE DO
         D=EXP(-X)
      END IF
      C1=ALOG10(C)
      D1=ALOG10(D)
      BCD=B1+C1+D1
      IF (BCD.LT.0.) THEN DO
         BCD=ABS(BCD)
         IF (BCD.GT.78) THEN DO
            DUMMYF=1.E-78
         ELSE DO
            TOP=B*C*D
            T1=ALOG10(TOP)
            T2=ALOG10(FACTN)
            T3=T1-T2
            IF(T3.LT.0..AND.ABS(T3).GT.78.) THEN DO
               DUMMYF=1.E-78
            ELSE DO
               DUMMYF=TOP/FACTN
            END IF
         END IF
      ELSE DO
         DUMMYF=B*C*D/FACTN
      END IF
C
C     ------------------------------------------------------------
C
      RETURN
      END
CNTRY
//FT11F001 DD DSN=dataset name,DISP=SHR
```